The Uncertainty Premium of Climate Tipping Points *

Andrea Titton †

December 31, 2025

Find latest version here.

*I am grateful to the Editor and Reviewers for their comments and suggestions. I thank Florian Wagener, Cees Diks, Rick van der Ploeg, Christoph Hambel, Frank Venmans, Luca Taschini, Simon Dietz, Philippa Johnson, Taco Prins, Sebastian Kreuzmair, and Niko Jaakkola for the insightful discussions.

†Department of Economics, University of Bologna

Abstract

Climate tipping points are shifts in the climate system that could lock the world into a higher-temperature regime. Many tipping points are characterised by Knightian uncertainty, that is, it is difficult to assign prior probabilities to their occurrence. This paper examines the economic costs of this Knightian uncertainty. To do so, I first derive optimal abatement policies for different tipping point scenarios using an integrated assessment model that includes temperature feedback effects. Then, I develop and compute a tipping point uncertainty premium on the social cost of carbon, as a function of different tipping point scenarios. I find that this premium on the social cost of carbon is between 12%-50% relative to complete-information scenarios. For tipping points triggered below 2.5° above pre-industrial levels, this uncertainty increases the social cost of carbon by between 20 and 40 US$ per tonne of carbon equivalent. Finally, I show that early discovery reduces the premium by 9%. This result illustrates that emission abatement policies in the coming decades are crucial in limiting tipping point risk, as early discovery might only offer moderate mitigation to the cost of uncertainty around tipping points.

As the global average temperature rises due to greenhouse gas emissions from human activities, temperature feedback mechanisms in the climate system can drive the world past tipping points, into a regime of higher temperatures. Unfortunately, tipping points are very hard (Ditlevsen and Ditlevsen, 2023; Ditlevsen and Johnsen, 2010; Rietkerk et al., 2025; Smolders, van Westen and Dijkstra, 2024), if not impossible (Ben-Yami et al., 2024), to predict, giving policymakers little to no time to react once they are crossed.

In this paper, I study the economic costs of Knightian uncertainty around climate tipping points. I address this uncertainty non-probabilistically by defining and computing a tipping point uncertainty premium on the social cost of carbon, as follows. Using an integrated assessment model that incorporates temperature feedback effects, I first compute optimal emissions abatement strategies across multiple tipping point scenarios calibrated to reflect recent evidence in the climate literature (Armstrong McKay et al., 2022; Deutloff, Held and Lenton, 2025; Seaver Wang et al., 2023). I then compute the indirect utility as a function of both the critical threshold T^c and temperature deviation ΔT^d at which the planner discovers the threshold. I use this indirect utility to compute the social cost of carbon, which I compare to the social cost of carbon under a complete-information benchmark. I interpret the difference in the social cost of carbon as the tipping point uncertainty premium. For simplicity, I hereafter referred to it as simply "uncertainty premium".

I show that the uncertainty premium on the social cost of carbon is between 12% and 50% relative to the complete-information benchmark. For critical thresholds below $2.5°$ above pre-industrial levels, this uncertainty increases the social cost of carbon by between 20 and 40 $\mathrm{US\$}$ per tonne of carbon equivalent (tCe). The greatest uncertainty premium occurs when the tipping point is triggered at around $2.1°$ with late discovery. Intuitively, if the tipping point occurs at higher temperatures, direct climate damages provide sufficient incentives to stabilise the climate before triggering the feedback. Conversely, if the tipping point occurs at lower temperatures, the costs of rapid abatement are

high, reducing the potential regret from late discovery. Finally, I show that early discovery has a moderately positive effect on the uncertainty premium: discovering the tipping point at a temperature level 1° lower leads to a 9% reduction in the social cost of carbon. This result cautions against postponing abatement, while relying on early discovery as a tool to prevent tipping points. These findings highlight that tipping elements should be treated carefully when studying the economic consequences of climate change, as small changes or modelling assumptions can lead to significant regret.

The rest of the paper is structured as follows. Section 1 puts the current paper in the context of the climate and environmental economic literature and highlights its contributions. Section 2 introduces the main components of the model: the climate, the economy, and the social planner problem. Section 3 computes optimal emissions abatement policies in a complete information benchmark, that is, when tipping points are known. Section 4 evaluates the costs of uncertainty by computing the social cost of carbon under different discovery scenarios and quantifies the value of early discovery. Finally, Section 5 draws policy implications and concludes.

1 Related Literature

A large body of recent economic literature has highlighted the importance of correctly incorporating climate dynamics when analysing the economic trade-off between current emissions and the reduction of future climate damages induced by rising temperatures. The key challenge is to develop integrated assessment models that, on the one hand, are sufficiently simple to be integrated into a dynamic optimisation problem, necessary to compute the economic costs of climate change and optimal emission abatement policies, and, on the other hand, can reproduce the key dynamics of larger, more accurate climate models (Dietz et al., 2021*a*). One dynamic aspect of the climate that has drawn much attention in economics is the concept of climate tipping points (Li, Crépin and Lindahl, 2024).

Early work on uncertain tipping points in environmental economics has modelled them using stochastic jump processes. Henceforth, I refer to this approach as *Barro disasters approach* as it builds on work on economic catastrophes by Barro (2009). At each moment in time, either temperature, atmospheric CO_2 concentration or climate damages to consumption experience a discontinuous jump with some probability known to the planner. This approach was introduced to climate economics by Pindyck and Wang (2013)[1]. It has been used in modelling climate tipping points by, for example, Lontzek et al. (2015), and Van der Ploeg and De Zeeuw (2018). The broad adoption of this approach is due to its flexibility as it allows for greater analytical tractability (Li, Crépin and Lindahl, 2024; Lin and Van Wijnbergen, 2023; Van den Bremer and Van der Ploeg, 2021), the introduction of uncertainty and ambiguity aversion (Olijslagers and Van Wijnbergen, 2019), and calibration (Hambel, Kraft and Schwartz, 2021). Nevertheless, this modelling choice neglects two crucial features of climate tipping points that are the focus of this paper. First, crossing a tipping point can push the climate into a new, persistent regime of high temperatures. Barro disasters are not suited to model these different regimes, as they model only transient catastrophic events. Second, it requires defining a probability distribution over the tipping event, whether real or the social planner's belief, which is, in reality, hard to compute reliably.

A second approach is to assume that with some state dependent probability either the marginal damages of temperature (Cai and Lontzek, 2019; Cai, Lenton and Lontzek, 2016) or the mapping between carbon concentration and temperature (Lemoine and Traeger, 2016*a*,*b*, 2014) change, such that the system dynamics follow a Markov chain. Henceforth, I refer to this approach as *Markov chain approach*. This model allows for irreversible tipping points, but displays two limitations. First, it requires an assumption about the distribution of the tipping point, or a prior over it. Lemoine and Traeger (2016*a*, 2014)

[1]This approach has an earlier history in the optimal control of environmental systems (Kamien and Schwartz, 1971; Nævdal and Oppenheimer, 2007; Tsur and Zemel, 1996, among others). I refer to Li, Crépin and Lindahl (2024, Section 3) for a detailed review.

take this to be uniform. This assumption might be too strong when dealing with rare events, such as tipping points. Second, in this literature, it is assumed that the planner can incorporate information from the climate and update their priors. This assumption might not be consistent with recent climate literature (Ben-Yami et al., 2024; Ditlevsen and Ditlevsen, 2023; Rietkerk et al., 2025) and possibly practically infeasible for many fast-moving systems (Rietkerk et al., 2025).

A third approach is to model feedback in climate dynamics explicitly. Hereafter, I refer to this as the *feedback approach*. This is closer to the real behaviour of the climate system (McGuffie and Henderson-Sellers, 2014), as it introduces multiple climate regimes, and is the standard one adopted in more complex climate modelling (e.g. Smith et al. 2017). Furthermore, optimisation over such systems has a long history in economics (Skiba, 1978) and has been developed extensively in environmental (Mäler, Xepapadeas and de Zeeuw, 2003; Wagener, 2013) and climate economics (Greiner and Semmler, 2005; Nordhaus, 2019; Wagener, 2015). Modelling the feedback explicitly has one drawback: it requires assuming the size of the feedback and when it comes into effect. These two properties are objects of empirical contention (Armstrong McKay et al., 2022; Seaver Wang et al., 2023). Furthermore, computationally solving such models can be technically challenging. Because of this, models of climate change with positive feedback are less commonly used when attempting to provide quantitative economic estimates via calibration.[2]

Lastly, a recent stream of literature (most notably Dietz et al. 2021*b*) circumvents the issue by foregoing the computation of optimal policies and embedding a simple and exogenous economic module into a complex climate model. Quantities of interest are then computed via *Monte Carlo* experiments. This approach allows economists to compute economic outcomes of climate tipping points by integrating state-of-the-art climate science, at the cost of not being

[2]As above, in this short paragraph, I have only focused on a few papers from this literature. I again refer the reader to Li, Crépin and Lindahl (2024, Section 4) for a more comprehensive review of the literature.

able to analyse counterfactual policies.

In this paper, I consider a tipping point induced by positive feedback in the temperature dynamics. I calibrate the feedback to match temperature dynamics in recent climate modelling of tipping points. I treat the Knightian uncertainty around the tipping point non-probabilistically and develop a novel measure of uncertainty premium in the social cost of carbon. The computation of the uncertainty premium builds on a long literature on the use of decision-theory rules, both probabilistic and non-probabilistic, in decision-making under Knightian uncertainty in climate economics (Athanassoglou and Xepapadeas, 2012; Heal and Millner, 2014; Millner, Dietz and Heal, 2013, among others). When dealing with Knightian uncertainty, there is a trade-off between a more informationally demanding probabilistic approach and a less information-demanding non-probabilistic approach (Heal and Millner, 2018). The former has been successfully employed to study tipping point uncertainty in climate economics (Lemoine and Traeger, 2016*a*; Traeger, 2014). The non-probabilistic approach taken here is then complementary to that of Lemoine and Traeger (2016*a*) as it gives a richer picture, that is, an upper bound on the uncertainty premium of tipping points on the social cost of carbon, but fewer policy prescriptions, such as what is the optimal abatement given our information today. This approach aligns with Heal (2017), who argues that climate policy must be grounded in aversion to risk and ambiguity, accounting for the small but positive risk of disastrous outcomes.

Finally, the numerical solver employed in the paper contributes to the literature on controlled stochastic processes by developing a parallelisation algorithm, based on Bierkens, Fearnhead and Roberts (2019), for the class of solvers introduced in Kushner and Dupuis (2001), and extending their results to recursive utilities.

2 Model

The following describes the climate and economic components of the model. First, Section 2.1.1 introduces carbon sinks and their interaction with atmospheric carbon concentration. Then, Section 2.1.2 defines the temperature dynamics and the temperature feedback mechanism that leads to a tipping point. Section 2.1.3 discusses the resulting tipping point in the climate system. Finally, Section 2.2 presents the economy.

2.1 Climate

2.1.1 Carbon sinks and $\mathrm{CO_2e}$ concentration

Emissions from human economic activity E_t increase the atmospheric concentration M_t of greenhouse gasses (GHGs), measured in their $\mathrm{CO_2}$ equivalent, hereafter $\mathrm{CO_2e}$. Part of this, in turn, decays into natural sinks. I denote by N_t the $\mathrm{CO_2e}$ concentration stored in natural sinks. As these sinks saturate, the rate of decay $\delta_m(N_t)$ depends on the stored $\mathrm{CO_2e}$ N_t. Hence, the stored $\mathrm{CO_2e}$ evolves as

$$\mathrm{d}N_t = \delta_m(N_t) M_t \, \mathrm{d}t. \tag{1}$$

This assumption on carbon sinks is in line with the empirical evidence and reflects the fact that it is much easier to stabilise atmospheric $\mathrm{CO_2e}$ concentration M_t if natural carbon sinks are not saturated, that is, for low values of N_t (Le Quéré et al., 2007; Shi et al., 2021).

In absence of abatement efforts, atmospheric $\mathrm{CO_2e}$ concentration M_t evolves according to the *no-policy* SSP5-8.5 scenario (Gidden et al., 2019). Variables under this scenario are indexed by the superscript np: let E_t^{np} be the no-policy emissions, and M_t^{np} and N_t^{np} the resulting atmospheric $\mathrm{CO_2e}$ concentration and the $\mathrm{CO_2e}$ stored in natural sinks, respectively. No-policy atmospheric $\mathrm{CO_2e}$ concentration M_t^{np} evolves as

$$\frac{\mathrm{d}M_t^{\mathrm{np}}}{M_t^{\mathrm{np}}} = \gamma_t^{\mathrm{np}} \mathrm{d}t + \sigma_m \mathrm{d}W_{m,t}, \tag{2}$$

where the no-policy expected growth rate of atmospheric CO_2e concentration is given by

$$\gamma_t^{\text{np}} := \frac{E_t^{\text{np}}}{M_t^{\text{np}}} - \delta_m(N_t^{\text{np}}) \tag{3}$$

and $W_{m,t}$ is a standard Brownian motion. The Brownian motion accounts for possible uncontrolled and unexpected shocks to CO_2e concentration, such as fluctuations in the absorption capacity of carbon sinks (DeVries et al., 2019). The variance σ_m^2 of these shocks is assumed to be constant. The no-policy scenario describes an energy intensive future, in which fossil fuel usage develops rapidly and little to no abatement takes place. I calibrate the implied growth rate of CO_2e concentration γ_t^{np}, using the projected CO_2e concentration path M_t^{np} from Gidden et al. (2019). The calibration is described in Appendix A.1.1 and its results are shown in Figure 1. The left figure shows the path of the

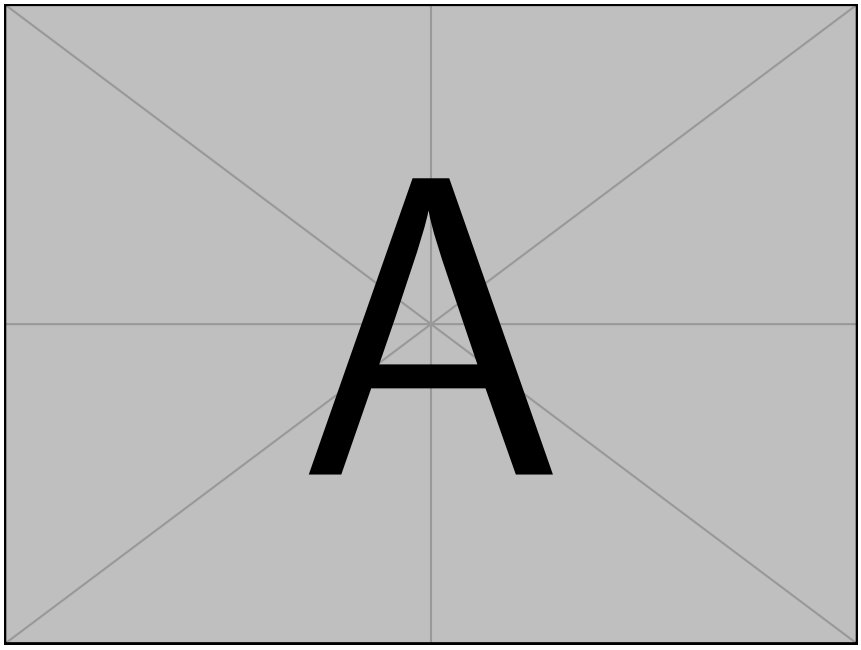

Figure 1: Growth rate of CO_2e concentration in the no-policy scenario γ_t^{np} and median path (solid) of no-policy CO_2e concentration M_t^{np} (2).

no-policy growth rate γ_t^{np} and the right figure shows the resulting growth of CO_2e concentration M_t^{np}. The CO_2e concentration in this scenario grows at an increasingly faster rate until approximately 2070, when the growth rate peaks just below 1.4%. Thereafter, the growth rate starts declining.

Abatement efforts α_t lower the growth rate of $\mathrm{CO_2e}$ concentration M_t vis-à-vis the no-policy scenario M_t^{np}. That is, the growth rate of $\mathrm{CO_2e}$ concentration M_t satisfies

$$\frac{\mathrm{d}M_t}{M_t} = \big(\gamma_t^{\mathrm{np}} - \alpha_t\big)\mathrm{d}t + \sigma_m \mathrm{d}W_{m,t}. \tag{4}$$

Implementing no abatement policy $\alpha_t = 0$ corresponds to a no-policy scenario $M_t = M_t^{\mathrm{np}}$, while implementing a full abatement policy $\alpha_t = \gamma_t^{\mathrm{np}}$ stabilises $\mathrm{CO_2e}$ concentration. Any abatement policy α_t can be linked to the implied level of emissions by introducing the emission reduction rate $\varepsilon(\alpha_t)$, which keeps tracks of what fraction of emissions is being abated

$$E_t = \big(1 - \varepsilon(\alpha_t)\big)E_t^{\mathrm{np}}. \tag{5}$$

Throughout the paper, policy results are reported in the faction of emissions abated $\varepsilon_t = \varepsilon(\alpha_t)$ rather than the abatement rate α_t. If abatement α_t exceeds the growth rate γ_t^{np} of $\mathrm{CO_2e}$ and the decay in carbon syncs $\delta_m(N_t)$, that is,

$$\alpha_t > \gamma_t^{\mathrm{np}} + \delta_m(N_t), \tag{6}$$

greenhouse gasses are sequestered from the atmosphere and atmospheric concentration M_t decreases. In this case, the fraction of abated emissions $\varepsilon_t > 1$.

2.1.2 Temperature

Average world temperature T_t [°] in deviation from pre-industrial levels is determined by a zero-dimensional energy balance model. Earth's energy balance, in its simplest form, prescribes that temperature tends towards balancing incoming solar radiation S and outgoing long-wave radiations $\eta\sigma T_t^4$, where σ is the Stefan-Boltzmann constant and η is an emissivity rate. Due to the presence of GHGs, certain wavelengths are scattered and not radiated outwards (Ghil and Childress, 2012). This introduces an additional radiative forcing G which yields the balance equation $S = \eta\sigma T_t^4 - G$. The GHGs radiative forcing term G can be decomposed into a constant component G_0 and a component which

depends on the equilibrium level of CO_2e concentration in the atmosphere M_t relative to the pre-industrial level M^p, such that

$$G = G_0 + G_1 \log(M_t/M^p). \tag{7}$$

The parameters G_0 and G_1 are calibrated to match the mapping between GHGs and temperature deviations in the FaIRv2 model (Leach et al., 2021). The calibration procedure is described in Appendix A.1.2. This zero-dimensional climate model does not capture the heterogeneity of temperature deviations and, as a consequence, climate damages, across the globe (McGuffie and Henderson-Sellers, 2014). Another limitation is that the temperature dynamics and the carbon cycle model are simpler than those commonly employed in the literature. Despite this, when targeting the average world temperature, the calibration presented here closely tracks the FaIRv2 projection (Leach et al., 2021) both in- and out-of-sample (see Figure 17 in Appendix A.1.2). Importantly, it closely tracks the timing of the temperature impulse response to an increase in atmospheric CO_2e concentration, which is a known limitation of climate modules in IAMs (Dietz et al., 2021*a*). I choose to match FaIRv2 projection as they are used in Deutloff, Held and Lenton (2025), which then serves as the basis for the tipping point calibration in this paper. Furthermore, the simple temperature dynamics allow us to solve for optimal closed-loop abatement policies, which are used to compute richer counterfactuals, as in Hambel, Kraft and Schwartz (2021). For an alternative approach to the study of tipping points, with a richer climate model but without optimal abatement policies, I refer the reader to Dietz et al. (2021*b*).

The climate system presents mechanisms that act as positive temperature feedbacks: an increase in global mean surface temperature can lead to additional forcing, which, in turn, further increases temperatures. For some of these mechanisms, the feedback is sufficiently strong that after a critical temperature level, referred to as a climate tipping point, the feedback becomes self-reinforcing and temperature increases to a hotter regime, even in the absence of

further GHG emissions from human activity. Such mechanisms are commonly referred to as tipping elements. Armstrong McKay et al. (2022) have identified nine salient global tipping elements in the context of climate change. The tipping elements which can potentially lead to the most significant warming are an abrupt permafrost collapse and the Amazon forest dieback. These tipping elements lead to an increase in emissions and, hence, radiative forcing as temperature rise (Parry, Ritchie and Cox, 2022; Turetsky et al., 2019). In this paper, I jointly model these tipping elements as an additional forcing factor $\lambda(T_t)$ which is increasing in temperature T_t (McGuffie and Henderson-Sellers, 2014). The function $\lambda(T_t)$ transitions from no additional forcing to an additional forcing level ΔS via a smooth transition function $L(T_t - T^c)$, that is,

$$\lambda(T_t) \coloneqq \Delta S \; L(T_t - T^c), \tag{8}$$

where T^c $[^\circ]$ is the critical temperature at which the feedback becomes self-reinforcing. The function L and the additional forcing ΔS are calibrated, in Appendix A.1.3, to match the additional warming caused by tipping elements in Deutloff, Held and Lenton (2025). An important distinction between the feedback mechanism presented here and that of Deutloff, Held and Lenton (2025) is that, in the latter, each tipping element is modelled as an additional positive mechanism that contributes to GHG emissions. This approach is more realistic than that taken in this paper and allows the authors to study interactions among various tipping elements. Nevertheless, the stylised formulation provided here is analytically tractable, while still capturing two key features of the results of Deutloff, Held and Lenton (2025). First, it captures the timing: once a tipping point is triggered, the additional warming is, on average, fully realised in 10.5 (± 4.64) years. Second, it captures the magnitude, as the average additional warming peaks at 0.8 $(\pm 0.3)^\circ$.

The only parameter which is not calibrated is the threshold temperature T^c[3]. Best estimates from climate sciences are that most relevant transitions

[3]In the simulations by Deutloff, Held and Lenton (2025), the authors sample uniformly on

occur for temperatures T_t between $2°$ and $4°$ over pre-industrial levels (Armstrong McKay et al., 2022; Seaver Wang et al., 2023). A large body of literature has focused on estimating critical thresholds associated with climate tipping points (e.g. Boulton, Allison and Lenton 2014; Van Westen, Kliphuis and Dijkstra 2024). However, for many climate feedback mechanisms, this can be very hard, if not impossible, to do (Ben-Yami et al., 2024; Ditlevsen and Ditlevsen, 2023; Ditlevsen and Johnsen, 2010; Rietkerk et al., 2025; Wagener, 2013). In line with this, to avoid attaching an arbitrary prior over the critical threshold T^c, in this paper I assume the uncertainty in T^c to be Knightian and employ a non-probabilistic decision-theoretic method to evaluate costs on the set of possible values $2° < T^c < 4°$. Figure 2 shows the calibrated transition function (8) under the two most extreme tipping point scenarios, and the linear model. De-

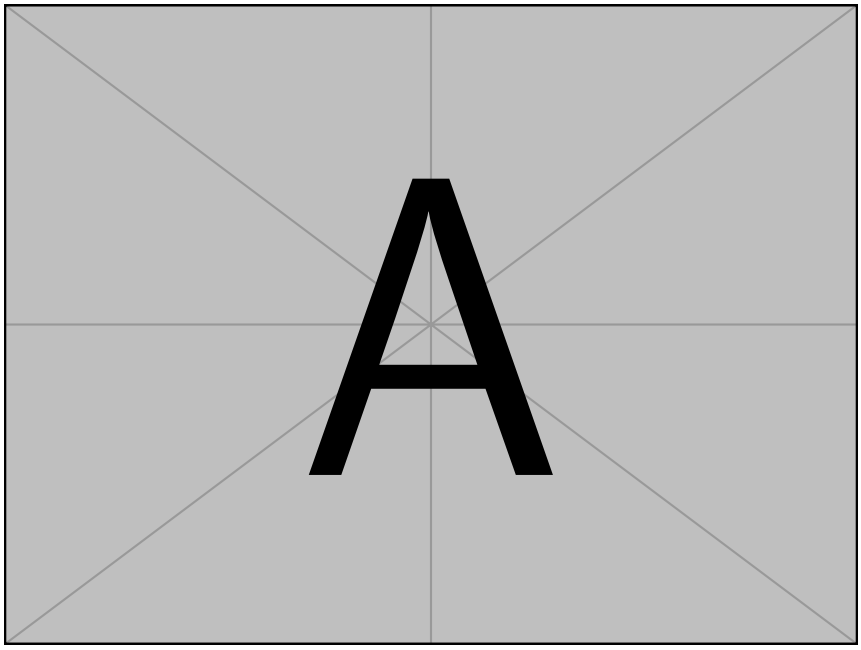

Figure 2: Temperature feedback $\lambda(T_t)$ in the $T^c = 2°$ and the $T^c = 4°$ scenario.

spite being a highly stylised and reduced form representation of a complex and spatially heterogeneous process, λ captures the core mechanism behind feedback processes in the temperature dynamics that can generate tipping points (McGuffie and Henderson-Sellers, 2014). This simple temperature feedback allows us to discuss and estimate the costs of transitioning to a new regime, what

the possible critical threshold ranges provided in Armstrong McKay et al. (2022)

ought to be (or not be) done to prevent this from happening, and the cost associated with the uncertainty around the tipping point.

Putting these processes together we can write down the two determinants of temperature dynamics: radiative forcing, which only depends on temperature,

$$r(T_t) \coloneqq S_0 \left(1 - \lambda(T_t)\right) - \eta\sigma T_t^4 \tag{9}$$

and the greenhouse gas effect, which only depends on the deviation of atmospheric $\mathrm{CO_2e}$ concentration to its pre-industrial level,

$$g(M_t) \coloneqq G_0 + G_1 \log(M_t/M^p). \tag{10}$$

Under these two drivers, temperature changes are given by

$$\epsilon \mathrm{d}T_t = r(T_t)\mathrm{d}t + g(M_t)\mathrm{d}t + \sigma_T \, \mathrm{d}W_{T,t}, \tag{11}$$

where ϵ is Earth's total heat capacity and $W_{T,t}$ is a Brownian motion, modelling uncontrolled shocks to temperature, which are assumed to have constant variance σ_T^2 and be uncorrelated with shocks $W_{m,t}$ to atmospheric $\mathrm{CO_2e}$ concentration.

2.1.3 Temperature Dynamics with a Tipping Point

The presence of the temperature feedback λ introduces a tipping point. In the following, I discuss the consequences of this tipping point for the temperature dynamics.

For a given level of $\mathrm{CO_2e}$ concentration M_t, the temperature T_t tends towards an equilibrium $\bar{T}$ that gives radiative balance in the temperature dynamics (11), that is,

$$r(\bar{T}) = -g(M_t). \tag{12}$$

The temperature feedback yields a climate with multiple regimes. That is, for the same level of atmospheric $\mathrm{CO_2e}$ concentration M_t, there are multiple lev-

els of temperature $\bar{T}$ which are in equilibrium. Figure 3 shows the equilibria of temperature (solid lines) as a function of $\mathrm{CO_2e}$ concentration when $T^c = 4°$ (darkest line), when $T^c = 2°$ (lighter line), and when there is no temperature feedback λ (lightest line). Without temperature feedback λ, the equilibrium

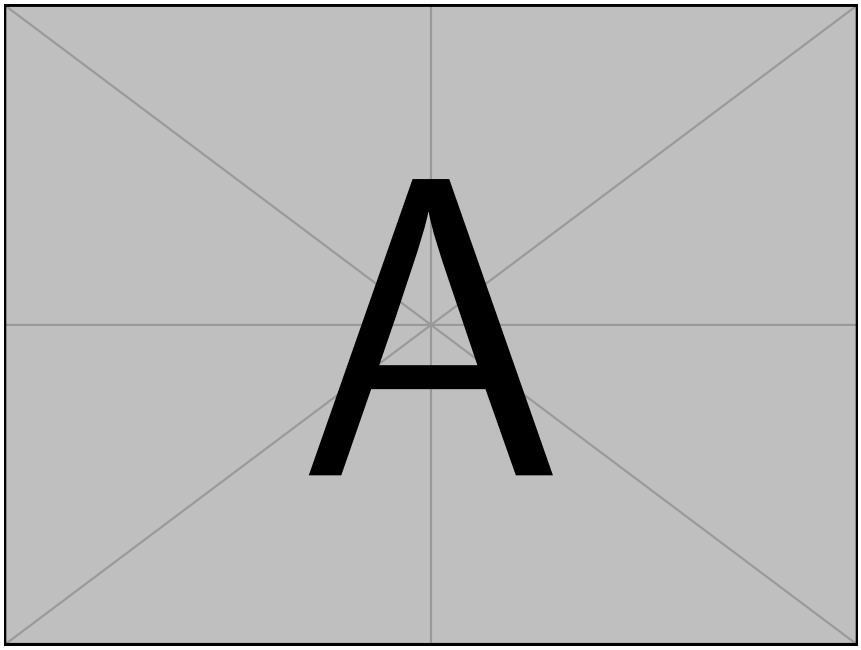

Figure 3: Equilibria of temperature T_t and $\mathrm{CO_2e}$ concentration M_t for $T^c = 2°$ (darker line), $T^c = 4°$ (darkest line), and no temperature feedback λ (lightest line). The solid lines show attracting equilibria and the dashed lines show repelling equilibria.

temperature is unique, and it rises with the logarithm of $\mathrm{CO_2e}$ concentration. If a temperature feedback λ is introduced there are two possible temperature regimes: a low temperature regime and a high temperature regime. These co-exist for some values of $\mathrm{CO_2e}$ concentration (dashed lines). In the $T^c = 2°$ scenario, for a $\mathrm{CO_2e}$ concentration M_t approximately at 550 p.p.m. both a low temperature regime, with $T_t < 2°$, and a high temperature regime, with $T_t > 2°$ are possible. In the $T^c = 4°$ scenario this phenomenon occurs only when $\mathrm{CO_2e}$ concentration M_t is approximately 950 p.p.m.. In a low temperature regime, the presence of a high temperature regime is hard to detect as the relationship between temperature T_t and $\mathrm{CO_2e}$ concentration M_t is not affected before the temperature feedback comes into effect.[4] If $\mathrm{CO_2e}$ concentration M_t increases

[4]Technically, the stable manifold of the model without feedback is a contact element of the stable manifold in the case with feedback.

and temperature crosses the critical threshold T^c, the old stable and low temperature regime is no longer feasible and only a high stable temperature regime remains. Then, any increase of $\mathrm{CO_2e}$ concentration pushes the system past a tipping point and temperature rapidly converges to the high temperature equilibrium. Crucially, to revert the system back to the lower temperature regime, it is not sufficient to remove just the carbon that caused the system to tip, but it is necessary to remove all carbon until the only stable equilibrium is the low temperature. In Figure 3, this would amount to bringing carbon back to $M_t < 550$, where the high temperature regime (solid black line) vanishes.

We can now ask what path of temperature T_t we would observe in these three scenarios if no abatement is implemented and $\mathrm{CO_2e}$ concentration M_t grows at the no-policy rate γ_t^{np}, such that $M_t = M_t^{\mathrm{np}}$. This is illustrated in Figure 4, which shows the median path over 50 years (marked line) of temperatures T_t and $\mathrm{CO_2e}$ concentration M_t under no-policy for the model without feedback and the two tipping scenarios, $T^c = 4°$ and $T^c = 2°$. Each marker is the outcome at the beginning of each decade. The simulations are overlaid onto the equilibria from Figure 3. In the case of $T^c = 2°$ (darkest line), the temperature deviates from the other scenarios by 2030. In case of $T^c = 4°$, temperature growth cannot be distinguished from a situation without temperature feedback and the two diverge only starting in 2050. In both cases, once the tipping point is crossed and the only regime is the high temperature one, temperature grows quickly to the new equilibrium. After that, the linear relationship between temperature and (log) $\mathrm{CO_2e}$ concentration is restored.

2.2 Economy

This section introduces the economy. The model assumes an AK economy, following Pindyck and Wang (2013), and Hambel, Kraft and Schwartz (2021).

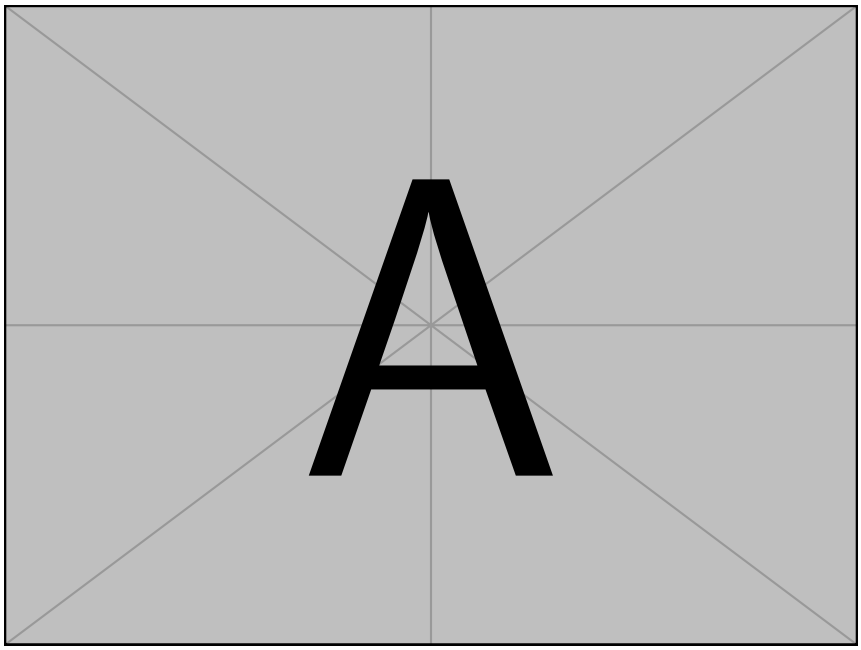

Figure 4: Median temperature T_t and CO_2e concentration M_t at time t of 100,000 simulations in case of no feedback (lightest line), $T^c = 4°$ (darker line), and $T^c = 2°$ (darkest line). The simulations are generated under the temperature dynamics (11) and the no-policy CO_2e concentration (2). Each marker is the value at the beginning of each decade. The thinner lines represent the equilibrium relationships as in Figure 3.

2.2.1 Climate Damages and Abatement Costs

Output Y_t, in trillion of US \$ per year, is the product of the capital stock K_t and its productivity A_t, that is,

$$Y_t = A_t K_t. \tag{13}$$

Climate change affects the economy by changing productivity growth $\frac{\mathrm{d}A_t}{\mathrm{d}t}$ via a damage function $d(T_t)$, which is otherwise assumed to grow at a constant exogenous rate ϱ, that is,

$$\frac{\mathrm{d}A_t}{\mathrm{d}t} = \varrho - d(T_t). \tag{14}$$

This is in line with recent empirical evidence on the channels by which warming affects the economy (Burke, Hsiang and Miguel, 2015; Dell, Jones and Olken, 2012; Kalkuhl and Wenz, 2020). Damages to productivity growth have been shown in the agricultural (Dietz and Lanz, 2019) and manufacturing sectors (Dell, Jones and Olken, 2009, 2012). Further discussion on this assumption is provided in Appendix A.2.3. I employ the global damage function estimated

by Kalkuhl and Wenz (2020, Section 6.2) and, hence, assume the damages to be quadratic in temperature T_t increases with respect to preindustrial level, that is,

$$d(T_t) := \xi T_t^2. \tag{15}$$

The damage function is displayed in Figure 5.

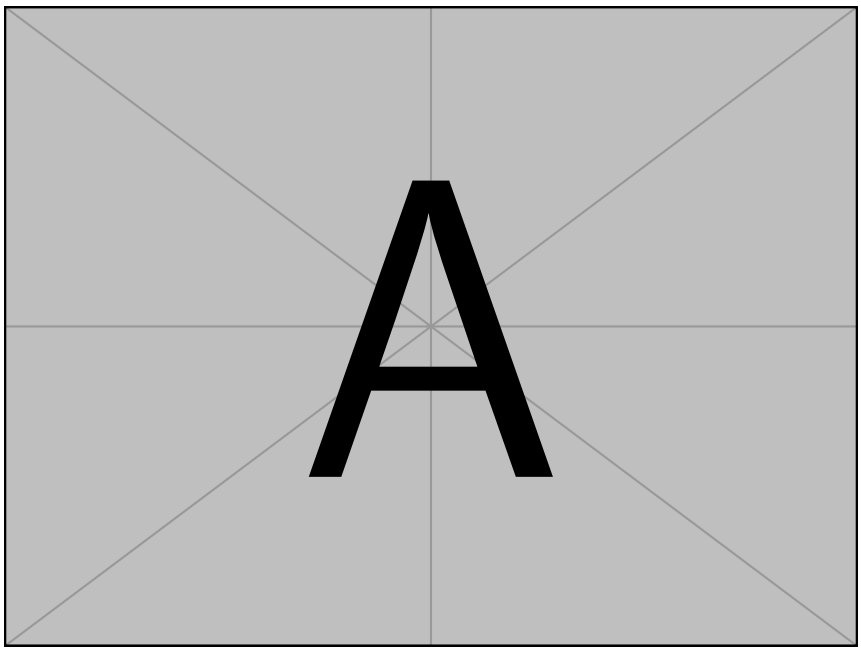

Figure 5: Damage function with the Kalkuhl and Wenz (2020) calibration.

Output Y_t can be used for investment in capital I_t, abatement expenditures B_t, or consumption C_t. This entails the budget constraint

$$Y_t = I_t + B_t + C_t. \tag{16}$$

Capital K_t depreciates at a rate δ_k but can be substituted by capital investments I_t, which are subject, along with abatement expenditure B_t, to quadratic adjustment costs

$$\frac{\kappa}{2}\left(\frac{I_t + B_t}{K_t}\right)^2 K_t. \tag{17}$$

Combining these, the endogenous growth of capital satisfies

$$\frac{\mathrm{d}K_t}{K_t} = \left(\frac{I_t}{K_t} - \delta_k - \frac{\kappa}{2} \left(\frac{I_t + B_t}{K_t} \right)^2 \right) \mathrm{d}t + \sigma_k \mathrm{d}W_{k,t}, \tag{18}$$

where $W_{k,t}$ is a standard Brownian motion.

In the following, I link the abatement costs B_t with the abatement rate α_t, introduced in the previous section. Define $\beta_t \coloneqq B_t/Y_t$ to be the fraction of output devoted to abatement. I assume this to be a power function of the fraction of abated emissions $\varepsilon(\alpha_t)$ (5), namely,

$$\beta_t(\varepsilon(\alpha_t)) = \omega_t \, \varepsilon(\alpha_t)^b. \tag{19}$$

Under this assumption, no abatement is free, as $\beta_t(0) = 0$. At a fixed time t, a higher abatement rate α_t and hence a higher emission reduction $\varepsilon(\alpha_t)$ vis-à-vis the no-policy scenario, becomes increasingly costly at rate

$$\beta_t'(\varepsilon(\alpha_t)) = b \, \omega_t \, \varepsilon(\alpha_t)^{b-1}. \tag{20}$$

It is common in the literature to assume the marginal abatement costs to be proportional to output and a power function in the abatement efforts (Baker, Clarke and Shittu, 2008; Dietz and Venmans, 2019; Hambel, Kraft and Schwartz, 2021; Nordhaus, 1992, 2017). As noted by Dietz and Venmans (2019, p.112-113), the proportionality with output arises because higher output growth increases energy demand. This must be satisfied with low-carbon energy technology which displays decreasing marginal productivity.

As time progresses, so does abatement technology and a given abatement objective becomes cheaper, as a fraction of output. This is modelled by letting the exogenous technological parameter ω_t decrease exponentially over time

$$\omega_t = \omega_0 e^{-\rho_\omega t}, \tag{21}$$

at a rate ρ_ω. The parameters ρ_ω and ω_0 are calibrated to match the implied

marginal abatement curves in the Sixth Assessment Report of the IPCC (2023*b*, Figure 3.33). More details on the calibration procedure can be found in Appendix A.2.2. The resulting abatement curves are displayed in Figure 6. The

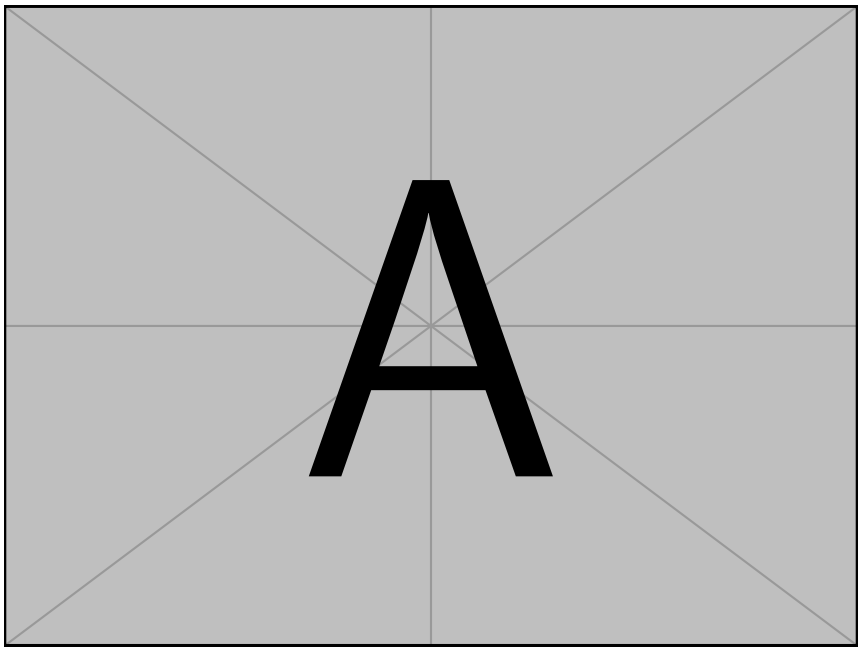

Figure 6: Calibrated abatement curves $\beta_t'(\varepsilon)$ for different times t.

shaded area represents the costs associated with abating more than 100% of the no-policy emissions. In this case, CO_2e is sequestered from the atmosphere.

Finally, let

$$\chi_t \coloneqq \frac{C_t}{Y_t} \tag{22}$$

be the fraction of output devoted to consumption. Using the budget constraint (16) and the two controlled rates, the abatement efforts α_t and the consumption rate χ_t, the growth rate of output can be rewritten, in terms of growth rates, as

$$\frac{\mathrm{d}Y_t}{Y_t} = \Big(\underbrace{\varrho + \phi_t(\chi_t)}_{\text{growth}} - \overbrace{A_t \beta_t(\varepsilon(\alpha_t))}^{\text{abatement}} - \underbrace{d(T_t)}_{\text{climate}} \Big) \mathrm{d}t + \sigma_k \mathrm{d}W_{k,t}, \tag{23}$$

where

$$\phi_t(\chi_t) \coloneqq A_t(1-\chi_t) - \frac{\kappa}{2} A_t^2 (1-\chi_t)^2 - \delta_k \tag{24}$$

is an endogenous growth component, $\beta_t(\varepsilon(\alpha_t))$ is the fraction of output allo-

cated to abatement for an abatement rate α_t, and $d(T_t)$ are the damages from climate change.

This formulation models the trade-off between climate abatement and economic growth. On the one hand, devoting fewer resources to abatement (lower α_t and, hence, $\beta_t(\varepsilon(\alpha_t))$) to pursue higher output growth, yields higher future temperature and can put the economy in a lower growth path altogether (higher $d(T_t)$). On the other hand, more ambitious abatement lowers future temperature and climate damages (lower $d(T_t)$), which boosts future economic growth, but costs economic growth today (higher α_t and, hence, $\beta_t(\varepsilon(\alpha_t))$).

3 Optimal Abatement Under complete-information

Given the climate and economic dynamics described in the previous section, I introduce the objective and optimal policies of a social planner who knows the tipping point location. I refer to this case as a "complete-information". Beyond the Knightian uncertainty in the tipping point, there is risk in the model, as temperature T_t, carbon concentration M_t, and output Y_t are subject to shocks. In the paper, this risk is fully quantifiable and the social planner, under complete-information, can maximise the average stream of utility. To account for relative risk aversion and intertemporal elasticity substitution the utility is recursively defined using the Epstein-Zin aggregator (Duffie and Epstein, 1992). Formally, at time t given the state of temperature, CO_2e concentration, carbon in sinks, and output $X_t \coloneqq (T_t, M_t, N_t, Y_t)$, societal utility is recursively defined as

$$V_t(X_t) = \sup_{\chi,\alpha} \mathbb{E}_t \int_t^\infty f(\chi_s(X_s)Y_s, V_s(X_s))\mathrm{d}s, \tag{25}$$

where χ and α are continuous policies over time and the state space, and f is the Epstein-Zin aggregator

$$f(C,V) \coloneqq \rho \frac{(1-\theta)\,V}{1-1/\psi}\left(\left(\frac{C}{((1-\theta)V)^{\frac{1}{1-\theta}}}\right)^{1-1/\psi} - 1\right). \tag{26}$$

This aggregator plays a dual role. First, it disentangles the role of relative risk aversion θ, elasticity of intertemporal substitution ψ, and the discount rate ρ in determining optimal abatement paths. Second, it circumvents the known paradoxical result that abatement policies become less ambitious as society becomes more risk averse (Pindyck and Wang, 2013).

Following the baseline formulation in Hambel, Kraft and Schwartz (2021), I set $\rho = 1.5\%$, $\theta = 10$ and $\psi = 1$. There is no consensus around the calibration of these parameters. I refer the reader to Pindyck and Wang (2013, Section 2), for a detailed discussion on the calibration of the preference parameters, and to Hambel, Kraft and Schwartz (2021) for their role in determining optimal abatement. Furthermore, the formulation assumes that preferences are stable over time, both in the parameters θ, ψ, and ρ and in their depending only on the consumption stream C_t. Future society might exhibit different preferences, for example, there might be an inherent utility from lower $\mathrm{CO_2e}$ concentration or temperature levels. For a discussion on incorporating this possibility in the analysis I refer the reader to Le Kama and Schubert (2004).

The social planner problem (25) is solved numerically. For more details, see Appendix B. The numerical solution relies on three steps. First, I derive the Hamilton-Jacobi-Bellman equation for the value function of the social planner V_t (25) and show that it can be factorised in an output dependent component Y_t and a cost function $F_t(T_t, M_t)$, which satisfies an auxiliary Hamilton-Jacobi-Bellman equation[5]. Second, in Section B.3, I derive an approximating Markov chain, that is, a discretisation of the state space T_t, M_t and a discrete Markov chain F_t^h over the discretisation, parametrised by a small step $h > 0$. I show that the recursive definition for F_t^h converges to the Hamilton-Jacobi-Bellman equation as $h \to 0$. This step extends the method developed by Kushner and Dupuis (2001) to a problem with recursive utility. Third, to compute the discretised cost function F_t^h, I assume that at $t = \tau = 500$, full abatement is

[5]This factorisation comes from the homogeneity of the Epstein-Zin aggregator f in Y, and it is commonly employed in the literature (Hambel, Kraft and Schwartz, 2021). I thank Christoph Hambel for pointing this out to me.

achieved $\alpha_\tau = \gamma_\tau^{np}$ and compute the discretised terminal cost function F_τ^h by value function iteration. Finally, by backward induction, I compute the discretised cost function F_t^h and the optimal policies α_t, χ_t using their first-order conditions. The model was solved on the Snellius HPC cluster using a parallelisation technique based on Bierkens, Fearnhead and Roberts (2019). The method developed by Kushner and Dupuis (2001) and adapted here, discretises directly the recursive definition of the value function (25) rather than the Hamilton-Jacobi-Bellman equation, as it is commonly done in finite difference schemes[6]. Furthermore, heuristically, the method performs well in the presence of nonlinearities, such as the one displayed by the temperature dynamics (11), as it produces a discrete Markov chain, analogous to the discrete time one in Cai and Lontzek (2019), with time steps proportional to the drift's magnitude in the state dynamics, such that around the tipping point the discretisation is finer in time and, hence, more precise.

Under the preference parameter choices described above, the solution, given a critical threshold T^c, yields a closed-loop abatement policy function φ^{T^c} such that optimal abatement is given by

$$\alpha_t = \varphi^{T^c}(t, T_t, M_t). \tag{27}$$

For illustration purposes, in the following I show optimal policies and their consequences in two climate scenarios: a "tipping" climate with a critical threshold of $T^c = 2.5°$ and a "linear" climate without a tipping point. Figure 7 shows the fraction of abated emission ε_t resulting from the implementation of the optimal policy $\varphi^{2.5°}$ in the tipping climate (black curve) and the optimal policy $\overline{\varphi}$ in the linear climate (gray curve). In the Figure, the optimal fraction of abated emission ε_t is displayed as a function of the carbon concentration along the no-policy np path, that is, for a given level of CO_2e concentration M_t^{np}, I compute the associated equilibrium temperature T_t^{np} and the time t at which it would be

[6]The most common approach in the *feedback mechanism* literature is to rely on optimal vector fields if the state dynamics are deterministic and finite difference discretisations if the dynamics are stochastic (Kiseleva and Wagener, 2010; Kossioris, Loulakis and Souganidis, 2019)

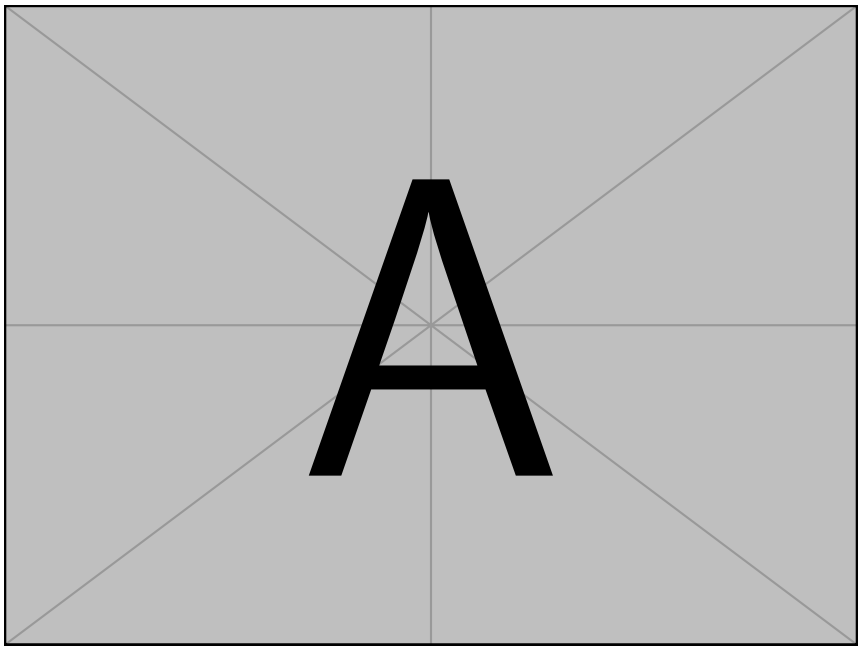

Figure 7: Fraction of abated emissions ε_t at different levels of $\mathrm{CO_2e}$ concentration M_t^{np} along the no-policy path np, for tipping climate (black curve) and linear climate (gray curve). The solid (dashed) line represents the policy before (after) crossing the critical threshold T^c. The shaded area represents negative emissions.

reached in the np scenario, hence, in absence of prior abatement efforts. Then the optimal fraction of abated emission $\varepsilon_t = \varepsilon(\varphi^{T^c}(t, T_t^{np}, M_t^{np}))$ is computed. In a tipping climate (black curve), the policy curve is solid for temperature values lower than the critical threshold T^c and dashed for temperature values larger the critical threshold T^c. In the presence of a tipping climate (black curve) the optimal fraction of abated emission ε_t responds more strongly to an increase $\mathrm{CO_2e}$ concentration, compared to a linear climate (gray curve). Once the tipping point is crossed abatement efforts are scaled back (post-tipping, dashed) as the climate is in a regime of high temperature. This result stems from the dual role of abatement: reducing first order climate damages and preventing the climate from tipping. Once the tipping point is crossed, the latter motive vanishes, and the marginal response of optimal abatement to an increase in $\mathrm{CO_2e}$ concentration is the same as in a linear climate (gray curve). This result echoes that of Clarke and Reed (1994), in which the authors shown that abatement efforts are scaled back once catastrophic risk becomes unavoidable.

The optimal abatement policies imply an optimal path of abatement ε_t and,

as a consequence, of $\mathrm{CO_2e}$ concentration M_t and temperature T_t. As the processes of $\mathrm{CO_2e}$ concentration (4) and temperature (11) are stochastic, so is the optimal path of abatement. In the following simulation, the median and 95% quantiles of the variables are computed by first simulating 100,000 paths under $\mathrm{CO_2e}$ concentration M_t (4) and temperature T_t (11) dynamics with optimal abatement policies $\alpha_t = \varphi^{T^c}(t, T_t, M_t)$. Then at each moment t, the relevant quantiles of each variable are computed, which yields a quantile path in t for each variable. Figure 8 shows the median path of the optimal fraction of abated emissions for the linear (left) and tipping (right) climate. In

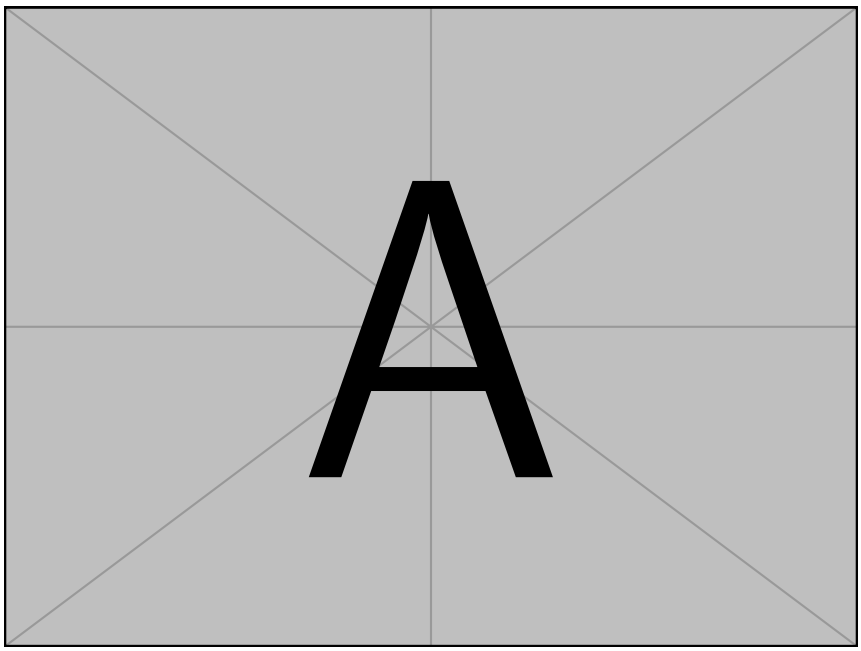

Figure 8: Median optimal abated fraction of emissions ε_t at time t of 100,000 simulations in a linear (left column) and a tipping climate (right column).

case of a linear climate, optimal abatement in 2020 is around 42% of the emissions in the no-policy benchmark, which corresponds to an emission level of around $37.35\mathrm{Gt\,CO_2e/year}$. Over time, abatement increases until full abatement is reached in 2072. Thereafter, abatement is further scaled up above 100%. In case of a tipping climate, optimal abatement rises more rapidly than in a linear climate, reacing 80% of abatement by 2040 and 100% of abatement by 2055, 17 years earlier than with a linear climate. Furthermore, negative abatement efforts are stronger and more prolongued. Figure 9 shows the resulting optimal

path of $\mathrm{CO_2e}$ variables in a linear (left panel) and a tipping (right panel) climate. The linear abatement policies cause $\mathrm{CO_2e}$ concentration M_t in the 2060s

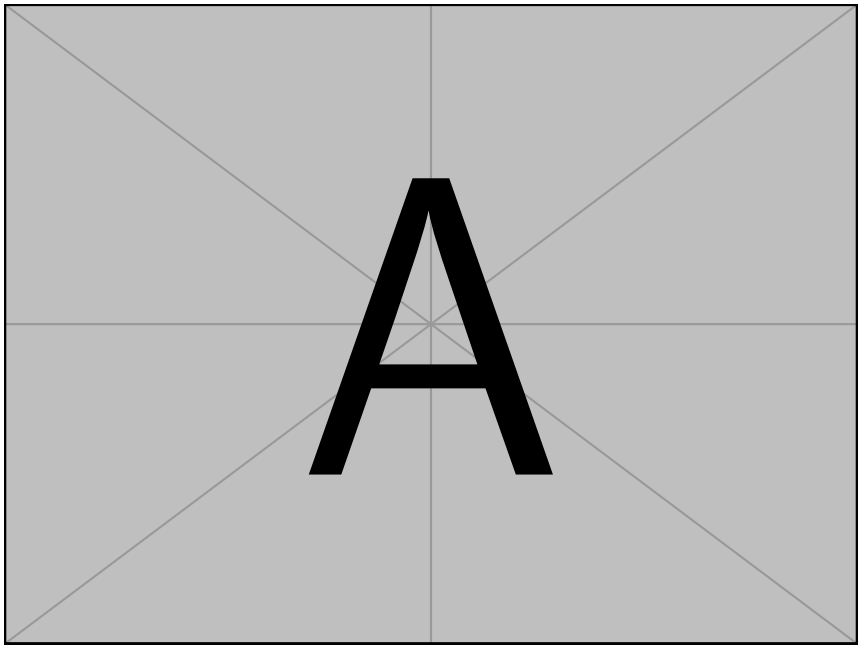

Figure 9: Median (solid) and 95 % simulation intervals (shaded area) abated fraction of emissions ε_t and temperature T_t at time t of 100,000 simulations in an imminent tipping point (left column) and a remote tipping point (right column). The simulations are generated under the temperature (11), $\mathrm{CO_2e}$ concentration (4), and output (23) dynamics with optimal abatement φ^{T^c}. The dashed line represents the median path in the no-policy scenario.

at aroud 560 ppm before starting to slowly decrease. As a consequence, temperature T_t in the median scenario are kept below 2° above pre-industrial levels. On the other hand, in a tipping climate, $\mathrm{CO_2e}$ concentration M_t peaks around 2050 below 540 $\mathrm{p.p.m.}$ and temperature T_t in the median scenario is kept well below 2° above pre-industrial levels, before converging back to around 1.5°. In the latter case, it is optimal for the social planner to quickly "slam the breaks" to avoid crossing a critical threshold and triggering a tipping point. Despite the tipping point not being triggered under optimal policies it still influences temperature T_t, as positive temperature shocks are more persistent. This can be seen in Figure 9 as the distribution of temperature is skewed towards higher temperatures whenever the climate is close to the tipping point, that is, between 2040 and 2060. Furthermore, once the tipping point is avoided, the planner keeps scaling up abatement efforts and stabilises temperatures around 1.5° to

move away from the critical temperature threshold, hence reducing the probability of a positive temperature shock triggering a tipping point.

The simulations in these two scenarios provide a qualitative description of the two scenarios, but to directly compare them it is necessary to take into account output growth and societal preferences. To do so, I compute the social cost of carbon (SCC) for the linear climate $\overline{\text{SCC}}$ and for the tipping climate SCC^{T^c} at different critical thresholds T^c. The SCC, measured in US\$ per tCe is the marginal rate of substitution between carbon equivalent emissions and output. This can also be interpreted as an optimal carbon tax and hence used to compare different climate regimes. In the context of our model, it can be computed as

$$\text{SCC}_t = -\frac{\partial V_t / \partial E_t}{\partial V_t / \partial Y_t}. \tag{28}$$

The left panel in Figure 10 shows the path of the SCC_t in a linear and a tipping climate. The right panel in Figure 10 shows the difference in median values of the two trajectories. Under both climates, the social cost of carbon

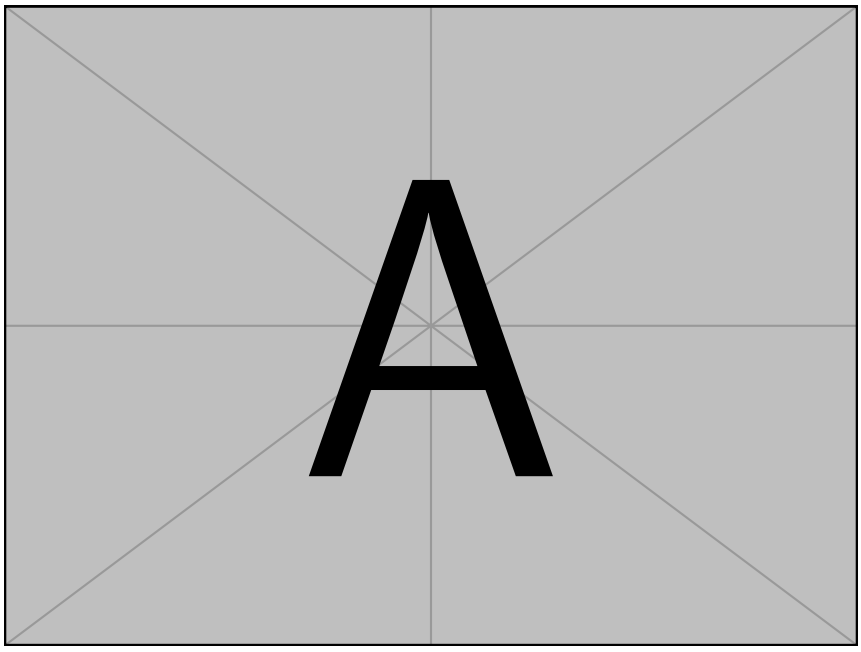

Figure 10: The left panel shows median (solid) and 95 % simulation intervals (shaded area) path of $\text{SCC}^{T^c=2.5^\circ}$ in a tipping climate and $\overline{\text{SCC}}$ in linear climate. The right panel shows the difference in medians $\text{SCC}^{T^c=2.5^\circ} - \overline{\text{SCC}}$.

grows rapidly from its initial value of around 80 US\$/tCe, driven by the in-

creased marginal damages of CO_2e emissions as temperature increases and output growth. The social cost of carbon in a tipping climate is higher throughout, reflecting the possibility of a tipping point being triggered. This difference grows rapidly between 2020 and 2080, when, in case of a tipping climate, the social planner quickly abates emissions to avoid triggering a tipping point. Thereafter, as the climate stabilises in both scenarios, the difference remains constant.

The social cost of a carbon at the start of the period, that is $t = 2020$, is a measure of the cost of tipping at different critical thresholds T^c. Figure 11 shows $\text{SCC}_{t=2020}^{T^c}$ as a function of different critical thresholds. The dashed line represents the social cost of carbon in a linear climate. First, the social cost of carbon

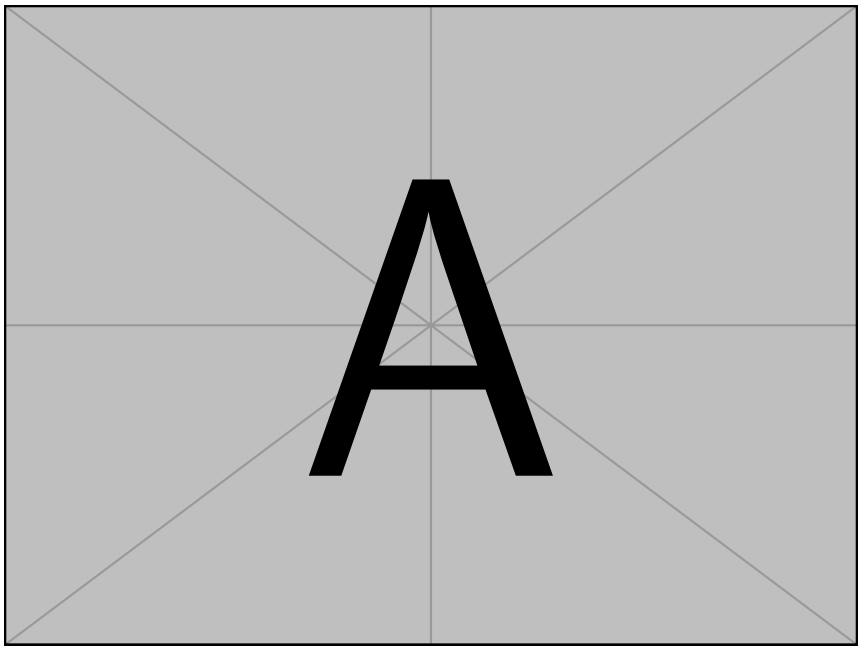

Figure 11: Social cost of carbon $\text{SCC}_t^{T^c}$ at the start of the period $t = 2020$, for different critical thresholds T^c. The dashed line represents the social cost of carbon in a linear climate.

$\text{SCC}_{t=2020}^{T^c}$ is strictly decreasing in the critical threshold T^c, as a higher critical threshold gives the social planner more time to abate. This effect is particulary pronounced for critical thresholds $T^c < 2.5°$ as, for higher critical thresholds, direct climate damages are sufficient incentives to optimally fully abate CO_2e emissions at temperature levels T_t lower than the critical threshold. Nevertheless, the presence of a tipping point, even if only triggered for large tem-

perature deviations T_t, yields a larger $\text{SCC}^{T^c}_{t=2020}$ compared to a linear climate, because there is always a probability that a large temperature shock triggeres a tipping point. As $T^c \to \infty$, this probability becomes vanishingly small and the social cost of carbon in a tipping cliamte converges to the linear one, that is, $\text{SCC}^{T^c}_t \to \overline{\text{SCC}}_t$. Second, the presence of a tipping point can significantly worsen the cost of climate change, as reflected in the $\text{SCC}^{T^c}_{t=2020}$ at the lowest threshold $T^c = 2°$ being approximately 40% larger than in the linear climate. Yet, the social cost of carbon is highly sensitive to the location of the critical threshold: a shift of $0.5°$ in T^c from $2°$ to $2.5°$ causes the social cost of carbon at $t = 2020$ to drop from 40% above the linear climate baseline to only around 2% above it. Hence, knowing the location of the critical threshold T^c is a major factor in optimally schedule abatement policies and small mistakes can lead to large consequences. Unfortunately, in the climate literature there is no consensus on whether we can predict such critical thresholds (Ben-Yami et al., 2024; Ditlevsen and Ditlevsen, 2023; Smolders, van Westen and Dijkstra, 2024), especially as the climate warms quickly due to anthropogenic greenhouse gasses emissions (Rietkerk et al., 2025).

4 Uncertainty Premium and the Value of Discovery

In this section, I focus on the uncertainty in the tipping element's critical threshold T^c. Given the aforementioned lack of consensus in the climate literature, I assume the planner cannot form a probabilistic prior over T^c. Instead, the planner evaluates the indirect utility associated with discovering the critical threshold at a temperature level $T^c + \Delta T^d$. If $\Delta T^d = 0$, the planner only discovers the critical threshold when the temperature reaches it. If $\Delta T^d < 0$, the planner discovers the critical threshold at lower temperature levels. Finally, if $\Delta T^d > 0$, the planner discovers the critical threshold at temperatures above it. In this section, I consider $-1° < \Delta T^d < +1°$ as a realistic range of early or late discovery. All other forms of risk, that is, those associated with economic W_k, CO_2e W_m, and temperature W_T shocks, are evaluated using the Epstein-Zin aggregator f.

Formally, let

$$\tau(T^c + \Delta T^d) \coloneqq \inf\left\{t : T_t \geq T^c + \Delta T^d\right\} \tag{29}$$

be the discovery time, that is, the time at which the planner discovers the location of the critical threshold. Then, the indirect utility of the planner, as a function of the critical threshold T^c and the discovery temperature deviation ΔT^d, can be written as

$$\begin{aligned} W_t(X_t; T^c, \Delta T^d) = \ & \mathbb{E}_0 \int_0^{\tau(T^c+\Delta T^d)} f(\overline{\chi}_s(X_s)Y_s, W_s(X_t; T^c, \Delta T^d))\mathrm{d}s \\ & + \int_{\tau(T^c+\Delta T^d)}^{\infty} f(\chi_s^{T^c}(X_s)Y_s, W_s(X_t; T^c, \Delta T^d))\mathrm{d}s \end{aligned} \tag{30}$$

where the dynamics of the state variables X_t are controlled by the linear abatement policy $\overline{\varphi}$ for $t < \tau(T^c + \Delta T^d)$ and with the optimal policy φ^{T^c} thereafter, that is, for $t \geq \tau(T^c + \Delta T^d)$. To illustrate how the discovery affects the trajectory of the state variables, Figure 12 shows the median path of $\mathrm{CO_2e}$ concentration M_t (top row) and temperature T_t (bottom row) under three discovery scenarios: early discovery at $\Delta T^d = -0.5^\circ$ (left column), discovery at the critical threshold $\Delta T^d = 0$ (center column), and late discovery at $\Delta T^d = 0.5^\circ$ (right column). In all three scenarios, $\mathrm{CO_2e}$ concentration peaks between 2060 and 2080 before declining, driven by negative emissions once the planner has discovered the critical threshold and switched to the optimal abatement policy φ^{T^c}. Early discovery at $\Delta T^d = -0.5^\circ$ enables the planner to limit the peak concentration to around 540 p.p.m. and stabilise temperature below 2°. In contrast, late discovery at $\Delta T^d = 0.5^\circ$ results in concentration peaking at 580 p.p.m. and temperature rising above 2°. Importantly, even in the case of late discovery $\Delta T^c = 0.5$, the tipping point is avoided, and temperature is stabilised at around 2°, albeit at the cost of a rapid emission reduction.

Using the indirect utility W, I compute the social cost of carbon

$$\mathrm{SCC}_t^{T^c, \Delta T^d} = -\frac{\partial W_t / \partial E_t}{\partial W_t / \partial Y_t}. \tag{31}$$

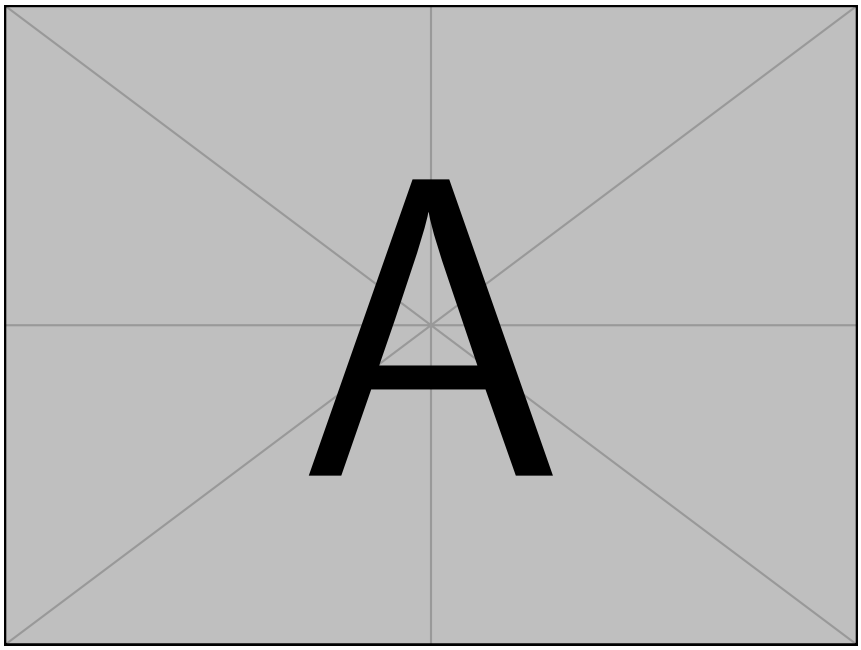

Figure 12: Median path of CO_2e concentration M_t (top row) and temperature T_t (bottom row) with 95% simulation intervals (shaded area) under different discovery scenarios ΔT^d. The dashed line represents the median trajectory under the no-policy. The simulations are generated under the temperature (11) and CO_2e concentration (4) dynamics with the critical threshold set at $T^c = 2.5°$.

This social cost of carbon incorporates an uncertainty premium associated with it, which I then use to estimate the cost of uncertainty. Before proceeding, I justify the non-probabilistic approach employed here. Relying on the indirect utility (30) is closely related to the minmax regret approach, advocated by Savage (1972), as the planner is computing the possible regret for each combination of critical thresholds T^c and discovery temperature ΔT^c. This approach is different yet complementary to the probabilistic approaches employed, for example, by Lemoine and Traeger (2016*a*, 2014). In the latter papers, the planner has a uniform prior over the possible values of the critical threshold T^c and updates it using Bayes' rule. Despite the usefulness of the latter approach, the one presented here remains agnostic about the planner's ability to incorporate information about the tipping point as temperature increases, a contentious issue in the climate literature (Ben-Yami et al., 2024; Ditlevsen and Ditlevsen, 2023; Rietkerk et al., 2025). Furthermore, given the possibly persistent effects of crossing a tipping point, the approach presented here avoids making strong assump-

tions about the distributional form of uncertainty when scientific consensus is lacking. I refer the reader to Heal and Millner (2014, 2018) for a more comprehensive discussion of the probabilistic and non-probabilistic decision-theoretic approaches employed in the literature on optimal control of the climate system.

To evaluate the cost of uncertainty, I now compute the $\mathrm{SCC}_{t=2020}^{T^c,\Delta T^d}$ (31) under the indirect utility W with discovery and compare it to the $\mathrm{SCC}_{t=2020}^{T^c}$ (28) under the optimal value function V. I interpret their difference as an "uncertainty premium", reflecting the planner's lack of complete information. Figure 13 shows the optimal $\mathrm{SCC}_{t=2020}^{T^c}$ (dashed) and the discovery $\mathrm{SCC}_{t=2020}^{T^c,\Delta T^d}$ (solid) as a function of the critical threshold T^c and the discovery temperature deviation ΔT^d. Figure 14 shows the percentage difference between the social cost of carbon un-

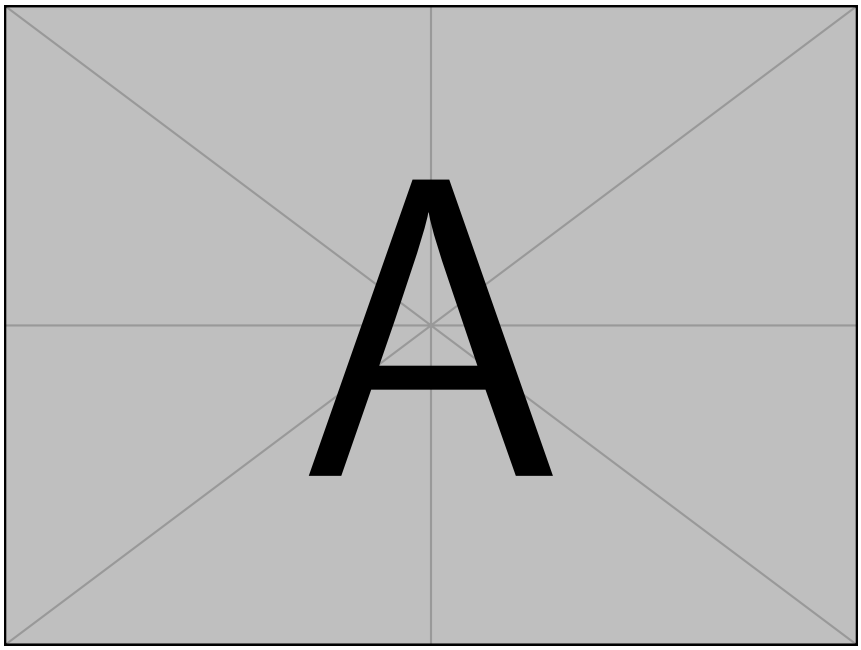

Figure 13: Social cost of carbon in 2020 as a function of the critical threshold T^c and discovery temperature deviation ΔT^d. The dashed line represents the optimal $\mathrm{SCC}_{2020}^{T^c}$ under complete information (28). The surface shows $\mathrm{SCC}_{2020}^{T^c,\Delta T^d}$ under uncertainty (31) for different combinations of T^c and ΔT^d.

der discovery $\mathrm{SCC}_{2020}^{T^c,\Delta T^d}$ and the optimal social cost of carbon $\mathrm{SCC}_{2020}^{T^c}$ across different values of the critical threshold T^c and discovery temperature deviation ΔT^d. First, the social cost of carbon under discovery $\mathrm{SCC}_{2020}^{T^c,\Delta T^d}$ is strictly increasing in late discovery, as discovering a tipping point at higher temperatures requires faster abatement, which, in turn, leads to higher abatement and

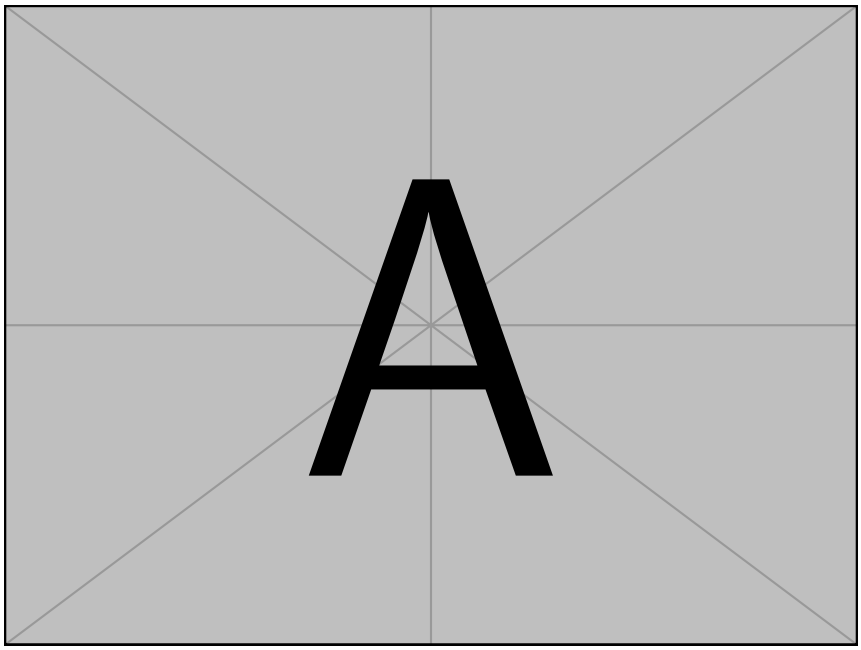

Figure 14: Percentage difference between the social cost of carbon under uncertainty and under complete information in 2020, as a function of the critical threshold T^c and discovery temperature deviation ΔT^d.

adjustment costs. Second, the uncertainty in the critical threshold T^c increases the social cost of carbon by at least 12%, from approximately 60 US$ per tCe to 90 US$ per tCe, and by at most 50% from 91 US$ per tCe to 137 US$. The largest percentage increase in the social cost of carbon is obtained in a late discovery $\Delta T^d = +1°$ of a tipping point with a critical threshold $T^c = +2.1°$. For such a tipping point, the relative cost of regret is the largest. On the one hand, for higher critical thresholds, late discovery is less harmful, since direct damages provide sufficient incentives to stabilise temperatures below the critical threshold. On the other hand, for lower critical thresholds, the proximity of the tipping point forces the planner to implement rapid, costly abatement, thereby reducing the potential regret of missing this opportunity.

Finally, I now turn to the question of how early discovery of the critical threshold affects the uncertainty premium. Figure 15 shows the social cost of carbon as a function of the critical threshold T^c for early discovery $\Delta T^d = -1°$ (gray) and contemporaneous discovery $\Delta T^d = 0$ (black), both in level terms (upper panel) and in percentage increase compared to the complete informa-

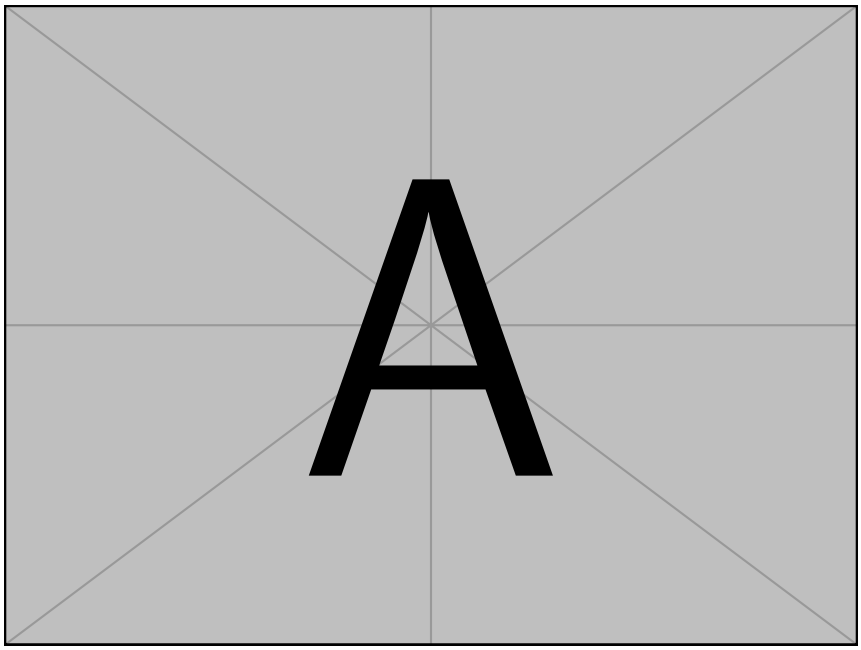

Figure 15: Social cost of carbon in 2020 as a function of the critical threshold T^c for early discovery ($\Delta T^d = -1°$, grey) and contemporaneous discovery ($\Delta T^d = 0$, black). The upper panel shows the level in $\mathrm{US\$}$ per tCe, while the lower panel shows the percentage increase compared to the complete information scenario.

tion scenario (lower panel). Early discovery lowers the uncertainty premium by, at most, 18.31 $\mathrm{US\$}$ per tCe, or approximately 9% relative to contemporaneous discovery. The benefit of early discovery is greatest for critical thresholds around $T^c = 2.1°$, where the uncertainty premium is most pronounced. For lower critical thresholds, the tipping point is sufficiently imminent that even contemporaneous discovery provides little additional cost relative to early discovery, as the planner must implement aggressive abatement regardless of discovery timing. For higher critical thresholds, the tipping point is sufficiently remote that direct climate damages dominate the decision to abate, rendering the timing of discovery less relevant. Hence, the moderate benefit of early discovery suggests that the primary driver of the uncertainty premium remains the fundamental unpredictability of tipping points, not merely the timing of their detection.

5 Discussion

This paper estimates the uncertainty premium on the social cost of carbon arising from uncertainty around climate tipping points. Temperature feedback is integrated in a state-of-the-art integrated assessment model, which is then calibrated. I address Knightian uncertainty about the tipping point in a non-probabilistic manner by evaluating the costs of discovering the tipping point's critical threshold at different temperature levels. I compute the indirect utility as a function of both the critical threshold and the temperature at which the planner discovers the threshold, then use this to estimate the tipping point uncertainty premium on the social cost of carbon.

I show that the premium relative to the complete-information benchmark is between 12% and 50%. This result demonstrates that feedback mechanisms in the climate system cannot be ignored when considering optimal abatement policies: by abating, we not only reduce future climate damages directly but also lower the likelihood of crossing a tipping point. Furthermore, I show that the greatest uncertainty premium occurs when the tipping point is triggered at around $2.1°$ of warming relative to the pre-industrial level with late discovery. Intuitively, if the tipping point occurs at higher temperatures, direct climate damages provide sufficient incentives to stabilise the climate before triggering the feedback. Conversely, if the tipping point occurs at lower temperatures, the costs of rapid abatement are high, reducing the uncertainty premium from late discovery. Nevertheless, for critical thresholds below $2.5°$ above pre-industrial levels, this uncertainty adds between 20 and 40 $\mathrm{US\$}$ per tCe to the social cost of carbon. Additionally, early discovery has a moderately positive effect on the uncertainty premium: discovering the tipping point at a temperature $1°$ lower reduces the social cost of carbon by approximately 9%. This moderate impact of early discovery on the uncertainty premium suggests that postponing emission abatement in the coming decades and relying on anticipating tipping points further down the line, can have large consequences in the presence of uncertain tipping point.

The approach employed in this paper complements that of Lemoine and Traeger (2016*a*), as both papers focus specifically on the additional costs induced by uncertainty about the tipping point. Lemoine and Traeger (2016*a*) employs a probabilistic approach to deal with the uncertainty in the tipping point and concludes that this leads to a moderate increase in the social cost of carbon of around 6%. In this paper, by employing a non-probabilistic approach and exploring various tipping-point scenarios and early or late discovery, I show that the uncertainty premium can be larger. This result suggests that errors in modelling climate tipping points can have large consequences for the social cost of carbon and highlights the need to account for climate tipping points when studying the overall economic consequences of climate change.

References

Ackerman, Frank, Elizabeth A. Stanton, and Ramón Bueno. 2013. "Epstein–Zin Utility in DICE: Is Risk Aversion Irrelevant to Climate Policy?" *Environmental and Resource Economics*, 56(1): 73–84. 53

Armstrong McKay, David I., Arie Staal, Jesse F. Abrams, Ricarda Winkelmann, Boris Sakschewski, Sina Loriani, Ingo Fetzer, Sarah E. Cornell, Johan Rockström, and Timothy M. Lenton. 2022. "Exceeding 1.5°C Global Warming Could Trigger Multiple Climate Tipping Points." *Science*, 377(6611): eabn7950. 3, 6, 12, 13, 52

Athanassoglou, Stergios, and Anastasios Xepapadeas. 2012. "Pollution control with uncertain stock dynamics: When, and how, to be precautious." *Journal of Environmental Economics and Management*, 63(3): 304–320. 7

Baker, Erin, Leon Clarke, and Ekundayo Shittu. 2008. "Technical Change and the Marginal Cost of Abatement." *Energy Economics*, 30(6): 2799–2816. 19

Barro, Robert J. 2009. "Rare Disasters, Asset Prices, and Welfare Costs." *American Economic Review*, 99(1): 243–264. 5

Ben-Yami, Maya, Andreas Morr, Sebastian Bathiany, and Niklas Boers. 2024. "Uncertainties Too Large to Predict Tipping Times of Major Earth System Components from Historical Data." *Science Advances*, 10(31): eadl4841. 3, 6, 13, 29, 31

Bierkens, Joris, Paul Fearnhead, and Gareth Roberts. 2019. "The Zig-Zag Process and Super-Efficient Sampling for Bayesian Analysis of Big Data." *The Annals of Statistics*, 47(3). 7, 23, 57, 66

Bondarev, Anton A., and Alfred Greiner. 2018. "Global Warming and Technical Change: Multiple Steady-States and Policy Options." *SSRN Electronic Journal*. 52

Boulton, Chris A., Lesley C. Allison, and Timothy M. Lenton. 2014. "Early Warning Signals of Atlantic Meridional Overturning Circulation Collapse in a Fully Coupled Climate Model." *Nature Communications*, 5(1): 5752–5752. 13

Burke, Marshall, Solomon Hsiang, and Edward Miguel. 2015. "Global Non-Linear Effect of Temperature on Economic Production." *Nature*, 527(7577): 235–239. 17, 55, 56

Byers, Edward, Volker Krey, Elmar Kriegler, Keywan Riahi, Roberto Schaeffer, Jarmo Kikstra, Robin Lamboll, Zebedee Nicholls, Marit Sandstad, Chris Smith, Kaj van der Wijst, Alaa Al -Khourdajie, Franck Lecocq, Joana Portugal-Pereira, Yamina Saheb, Anders Stromman, Harald Winkler, Cornelia Auer, Elina Brutschin, Matthew Gidden, Philip Hackstock, Mathijs Harmsen, Daniel Huppmann, Peter Kolp, Claire Lepault, Jared Lewis, Giacomo Marangoni, Eduardo Müller-Casseres, Ragnhild Skeie, Michaela Werning, Katherine Calvin, Piers Forster, Celine Guivarch, Tomoko Hasegawa, Malte Meinshausen, Glen Peters, Joeri Rogelj, Bjorn Samset, Julia Steinberger, Massimo Tavoni, and Detlef van Vuuren. 2022. "AR6 Scenarios Database." 54

Cai, Yongyang, and Thomas S. Lontzek. 2019. "The Social Cost of Carbon with Economic and Climate Risks." *Journal of Political Economy*, 127(6): 2684–2734. 5, 23, 65

Cai, Yongyang, Timothy M. Lenton, and Thomas S. Lontzek. 2016. "Risk of Multiple Interacting Tipping Points Should Encourage Rapid CO2 Emission Reduction." *Nature Climate Change*, 6(5): 520–525. 5

Clarke, Harry R., and William J. Reed. 1994. "Consumption/pollution tradeoffs in an environment vulnerable to pollution-related catastrophic collapse." *Journal of Economic Dynamics and Control*, 18(5): 991–1010. 24

Crost, Benjamin, and Christian P. Traeger. 2013. "Optimal Climate Policy: Uncertainty versus Monte Carlo." *Economics Letters*, 120(3): 552–558. 53

Dell, Melissa, Benjamin F Jones, and Benjamin A Olken. 2009. "Temperature and Income: Reconciling New Cross-Sectional and Panel Estimates." *American Economic Review*, 99(2): 198–204. 17

Dell, Melissa, Benjamin F Jones, and Benjamin A Olken. 2012. "Temperature Shocks and Economic Growth: Evidence from the Last Half Century." *American Economic Journal: Macroeconomics*, 4(3): 66–95. 17, 55

Deutloff, Jakob, Hermann Held, and Timothy M. Lenton. 2025. "High Probability of Triggering Climate Tipping Points under Current Policies Modestly Amplified by Amazon Dieback and Permafrost Thaw." *Earth System Dynamics*, 16(2): 565–583. 3, 11, 12, 50, 52

DeVries, Tim, Corinne Le Quéré, Oliver Andrews, Sarah Berthet, Judith Hauck, Tatiana Ilyina, Peter Landschützer, Andrew Lenton, Ivan D. Lima, Michael Nowicki, Jörg Schwinger, and Roland Séférian. 2019. "Decadal trends in the ocean carbon sink." *Proceedings of the National Academy of Sciences*, 116(24): 11646–11651. 9

Dietz, Simon, and Bruno Lanz. 2019. "Growth and Adaptation to Climate Change in the Long Run." IRENE Institute of Economic Research IRENE Working Papers 19-09. 17

Dietz, Simon, and Frank Venmans. 2019. "Cumulative Carbon Emissions and Economic Policy: In Search of General Principles." *Journal of Environmental Economics and Management*, 96: 108–129. 19

Dietz, Simon, Frederick van der Ploeg, Armon Rezai, and Frank Venmans. 2021*a*. "Are Economists Getting Climate Dynamics Right and Does It Matter?" *Journal of the Association of Environmental and Resource Economists*. 4, 11, 51

Dietz, Simon, James Rising, Thomas Stoerk, and Gernot Wagner. 2021*b*. "Economic Impacts of Tipping Points in the Climate System." *Proceedings of the National Academy of Sciences*, 118(34): e2103081118. 6, 11

Ditlevsen, Peter, and Susanne Ditlevsen. 2023. "Warning of a Forthcoming Collapse of the Atlantic Meridional Overturning Circulation." *Nature Communications*, 14(1): 4254. 3, 6, 13, 29, 31

Ditlevsen, Peter D., and Sigfus J. Johnsen. 2010. "Tipping Points: Early Warning and Wishful Thinking." *Geophysical Research Letters*, 37(19): 2010GL044486. 3, 13

Duffie, Darrell, and Larry G. Epstein. 1992. "Asset Pricing with Stochastic Differential Utility." *Review of Financial Studies*, 5(3): 411–436. 21

Ghil, Michael, and Stephen Childress. 2012. *Topics in Geophysical Fluid Dynamics: Atmospheric Dynamics, Dynamo Theory, and Climate Dynamics*. Vol. 60, Springer Science & Business Media. 10

Gidden, Matthew J., Keywan Riahi, Steven J. Smith, Shinichiro Fujimori, Gunnar Luderer, Elmar Kriegler, Detlef P. Van Vuuren, Maarten Van Den Berg, Leyang Feng, David Klein, Katherine Calvin, Jonathan C. Doelman, Stefan Frank, Oliver Fricko, Mathijs Harmsen, Tomoko Hasegawa, Petr Havlik, Jérôme Hilaire, Rachel Hoesly, Jill Horing, Alexander Popp, Elke Stehfest, and Kiyoshi Takahashi. 2019. "Global Emissions Pathways under Different Socioeconomic Scenarios for Use in CMIP6: A Dataset of Harmonized Emissions Trajectories through the End of the Century." *Geoscientific Model Development*, 12(4): 1443–1475. 8, 9, 48, 49

Greiner, Alfred, and Willi Semmler. 2005. "Economic Growth and Global Warming: A Model of Multiple Equilibria and Thresholds." *Journal of Economic Behavior & Organization*, 57(4): 430–447. 6

Guivarch, Céline, Thomas Le Gallic, Nico Bauer, Panagiotis Fragkos, Daniel Huppmann, Marc Jaxa-Rozen, Ilkka Keppo, Elmar Kriegler, Tamás Krisztin, Giacomo Marangoni, Steve Pye, Keywan Riahi, Roberto Schaeffer, Massimo Tavoni, Evelina Trutnevyte, Detlef van Vuuren, and Fabian

Wagner. 2022. "Using Large Ensembles of Climate Change Mitigation Scenarios for Robust Insights." *Nature Climate Change*, 12(5): 428–435. 50

Hambel, Christoph, Holger Kraft, and Eduardo Schwartz. 2021. "Optimal Carbon Abatement in a Stochastic Equilibrium Model with Climate Change." *European Economic Review*, 132: 103642. 5, 11, 16, 19, 22, 54, 56, 57

Heal, Geoffrey. 2017. "The Economics of the Climate." *Journal of Economic Literature*, 55(3): 1046–1063. 7

Heal, Geoffrey, and Antony Millner. 2014. "Reflections: Uncertainty and Decision Making in Climate Change Economics." *Review of Environmental Economics and Policy*, 8(1): 120–137. 7, 32

Heal, Geoffrey, and Antony Millner. 2018. "Chapter 10 - Uncertainty and ambiguity in environmental economics: conceptual issues." In *Handbook of Environmental Economics*. Vol. 4 of *Handbook of Environmental Economics*, , ed. Partha Dasgupta, Subhrendu K. Pattanayak and V. Kerry Smith, 439–468. Elsevier. 7, 32

Howard, Peter H., and Thomas Sterner. 2017. "Few and Not so Far between: A Meta-Analysis of Climate Damage Estimates." *Environmental and Resource Economics*, 68(1): 197–225. 55

IPCC. 2023*a*. *Climate Change 2021 – The Physical Science Basis: Working Group I Contribution to the Sixth Assessment Report of the Intergovernmental Panel on Climate Change.* . 1 ed., Cambridge University Press. 48

IPCC, ed. 2023*b*. *Climate Change 2022 - Mitigation of Climate Change: Working Group III Contribution to the Sixth Assessment Report of the Intergovernmental Panel on Climate Change.* . 1 ed., Cambridge University Press. 20, 54

Kalkuhl, Matthias, and Leonie Wenz. 2020. "The Impact of Climate Conditions on Economic Production. Evidence from a Global Panel of Regions." *Journal of Environmental Economics and Management*, 103: 102360. 17, 18, 55, 56

Kamien, Morton I., and Nancy L. Schwartz. 1971. "Sufficient Conditions in Optimal Control Theory." *Journal of Economic Theory*, 3(2): 207–214. 5

Kiseleva, Tatiana, and F.O.O. Wagener. 2010. "Bifurcations of optimal vector fields in the shallow lake model." *Journal of Economic Dynamics and Control*, 34(5): 825–843. 23

Kossioris, G. T., M. Loulakis, and P. E. Souganidis. 2019. "The Deterministic and Stochastic Shallow Lake Problem." *Probability and Analysis in Interacting Physical Systems*, 49–74. Springer International Publishing. 23

Kraft, Holger, and Frank Thomas Seifried. 2014. "Stochastic Differential Utility as the Continuous-Time Limit of Recursive Utility." *Journal of Economic Theory*, 151: 528–550. 63

Kushner, Harold J. 2007. "Numerical Approximations for Nonzero-Sum Stochastic Differential Games." *SIAM Journal on Control and Optimization*, 46(6): 1942–1971. 57, 62

Kushner, Harold J., and Paul Dupuis. 2001. *Numerical Methods for Stochastic Control Problems in Continuous Time.* Vol. 24 of *Stochastic Modelling and Applied Probability*, New York, NY:Springer New York. 7, 22, 23, 57, 62, 64

Leach, Nicholas J., Stuart Jenkins, Zebedee Nicholls, Christopher J. Smith, John Lynch, Michelle Cain, Tristram Walsh, Bill Wu, Junichi Tsutsui, and Myles R. Allen. 2021. "FaIRv2.0.0: A Generalized Impulse Response Model for Climate Uncertainty and Future Scenario Exploration." *Geoscientific Model Development*, 14(5): 3007–3036. 11, 50

Le Kama, Alain Ayong, and Katheline Schubert. 2004. "Growth, Environment and Uncertain Future Preferences." *Environmental and Resource Economics*, 28(1): 31–53. 22

Lemoine, Derek, and Christian P. Traeger. 2016*a*. "Ambiguous Tipping Points." *Journal of Economic Behavior & Organization*, 132: 5–18. 5, 7, 31, 36

Lemoine, Derek, and Christian P. Traeger. 2016*b*. "Economics of Tipping the Climate Dominoes." *Nature Climate Change*, 6(5): 514–519. 5

Lemoine, Derek, and Christian Traeger. 2014. "Watch Your Step: Optimal Policy in a Tipping Climate." *American Economic Journal: Economic Policy*, 6(1): 137–166. 5, 31

Le Quéré, Corinne, Christian Rödenbeck, Erik T. Buitenhuis, Thomas J. Conway, Ray Langenfelds, Antony Gomez, Casper Labuschagne, Michel Ramonet, Takakiyo Nakazawa, Nicolas Metzl, Nathan Gillett, and Martin Heimann. 2007. "Saturation of the Southern Ocean CO2 Sink Due to Recent Climate Change." *Science*, 316(5832): 1735–1738. 8

Li, Chuan-Zhong, Anne-Sophie Crépin, and Therese Lindahl. 2024. "The Economics of Tipping Points: Some Recent Modeling and Experimental Advances." *International Review of Environmental and Resource Economics*, 18(4): 385–442. 4, 5, 6

Lin, Xu, and Sweder Van Wijnbergen. 2023. "The Social Cost of Carbon under Climate Volatility Risk." Tinbergen Institute Tinbergen Institute Discussion Papers 23-032/IV. 5

Lontzek, Thomas S., Yongyang Cai, Kenneth L. Judd, and Timothy M. Lenton. 2015. "Stochastic Integrated Assessment of Climate Tipping Points Indicates the Need for Strict Climate Policy." *Nature Climate Change*, 5(5): 441–444. 5, 53

Mäler, Karl-Göran, Anastasios Xepapadeas, and Aart de Zeeuw. 2003. "The Economics of Shallow Lakes." *Environmental and Resource Economics*, 26(4): 603–624. 6

McGuffie, Kendal, and Ann Henderson-Sellers. 2014. *The Climate Modelling Primer*. . 4. ed ed., Chicester:Wiley Blackwell. 6, 11, 12, 13

Millner, Antony, Simon Dietz, and Geoffrey Heal. 2013. "Scientific Ambiguity and Climate Policy." *Environmental and Resource Economics*, 55(1): 21–46. 7

Mogensen, Patrick Kofod, and Asbjørn Nilsen Riseth. 2018. "Optim: A Mathematical Optimization Package for Julia." *Journal of Open Source Software*, 3(24): 615. 66

Nævdal, Eric, and Michael Oppenheimer. 2007. "The Economics of the Thermohaline Circulation—A Problem with Multiple Thresholds of Unknown Locations." *Resource and Energy Economics*, 29(4): 262–283. 5

Nordhaus, William D. 1992. "An Optimal Transition Path for Controlling Greenhouse Gases." *Science*, 258(5086): 1315–1319. 19

Nordhaus, William D. 2014. "Estimates of the Social Cost of Carbon: Concepts and Results from the DICE-2013R Model and Alternative Approaches." *Journal of the Association of Environmental and Resource Economists*, 1(1): 273–312. 53

Nordhaus, William D. 2017. "Revisiting the Social Cost of Carbon." *Proceedings of the National Academy of Sciences of the United States of America*, 114(7): 1518–1523. 19

Nordhaus, William D. 2019. "Economics of the Disintegration of the Greenland Ice Sheet." *Proceedings of the National Academy of Sciences*, 116(25): 12261–12269. 6

Nordhaus, William D., and Andrew Moffat. 2017. "A Survey of Global Impacts of Climate Change: Replication, Survey Methods, and a Statistical Analysis." National Bureau of Economic Research w23646, Cambridge, MA. 55

Oberkampf, William L., and Christopher J. Roy. 2010. *Verification and Validation in Scientific Computing*. Cambridge University Press. 65

Olijslagers, Stan, and Sweder Van Wijnbergen. 2019. "Discounting the Future: On Climate Change, Ambiguity Aversion and Epstein-Zin Preferences." *SSRN Electronic Journal*. 5

Parry, Isobel M., Paul D. L. Ritchie, and Peter M. Cox. 2022. "Evidence of Localised Amazon Rainforest Dieback in CMIP6 Models." *Earth System Dynamics*, 13(4): 1667–1675. 12

Pindyck, Robert S., and Neng Wang. 2013. "The Economic and Policy Consequences of Catastrophes." *American Economic Journal: Economic Policy*, 5(4): 306–339. 5, 16, 22, 56

Rackauckas, Christopher, and Qing Nie. 2017. "Adaptive Methods for Stochastic Differential Equations via Natural Embeddings and Rejection Sampling with Memory." *Discrete and continuous dynamical systems. Series B*, 22(7): 2731. 66

Rackauckas, Christopher, Yingbo Ma, Julius Martensen, Collin Warner, Kirill Zubov, Rohit Supekar, Dominic Skinner, and Ali Ramadhan. 2020. "Universal Differential Equations for Scientific Machine Learning." *arXiv preprint arXiv:2001.04385*. 48

Rietkerk, Max, Vanessa Skiba, Els Weinans, Raphaël Hébert, and Thomas Laepple. 2025. "Ambiguity of early warning signals for climate tipping points." *Nature Climate Change*, 15(5): 479–488. 3, 6, 13, 29, 31

Savage, L.J. 1972. *The Foundations of Statistics. Dover Books on Mathematics*, Dover Publications. 31

Seaver Wang, A. Foster, E. A. Lenz, J. Kessler, J. Stroeve, L. Anderson, M. Turetsky, R. Betts, Sijia Zou, W. Liu, W. Boos, and Z. Hausfather. 2023. "Mechanisms and Impacts of Earth System Tipping Elements." *Reviews of Geophysics*. 3, 6, 13

Shi, Hao, Hanqin Tian, Naiqing Pan, Christopher P. O. Reyer, Philippe Ciais, Jinfeng Chang, Matthew Forrest, Katja Frieler, Bojie Fu, Anne Gädeke, Thomas Hickler, Akihiko Ito, Sebastian Ostberg, Shufen Pan, Miodrag Stevanović, and Jia Yang. 2021. "Saturation of Global Terrestrial

Carbon Sink Under a High Warming Scenario." *Global Biogeochemical Cycles*, 35(10): e2020GB006800. 8

Skiba, A. K. 1978. "Optimal Growth with a Convex-Concave Production Function." *Econometrica*, 46(3): 527. 6

Smith, Christopher J., Piers M. Forster, Myles Allen, Nicholas Leach, Richard J. Millar, Giovanni A. Passerello, and Leighton A. Regayre. 2017. "FAIR v1.1: A Simple Emissions-Based Impulse Response and Carbon Cycle Model." 6

Smolders, Emma J. V., René M. van Westen, and Henk A. Dijkstra. 2024. "Probability Estimates of a 21st Century AMOC Collapse." 3, 29

Tol, Richard S.J. 2024. "A Meta-Analysis of the Total Economic Impact of Climate Change." *Energy Policy*, 185: 113922. 55

Traeger, Christian P. 2014. "Why uncertainty matters: discounting under intertemporal risk aversion and ambiguity." *Economic Theory*, 56(3): 627–664. 7

Tsur, Yacov, and Amos Zemel. 1996. "Accounting for Global Warming Risks: Resource Management under Event Uncertainty." *Journal of Economic Dynamics and Control*, 20(6-7): 1289–1305. 5

Turetsky, Merritt R., Benjamin W. Abbott, Miriam C. Jones, Katey Walter Anthony, David Olefeldt, Edward A. G. Schuur, Charles Koven, A. David McGuire, Guido Grosse, Peter Kuhry, Gustaf Hugelius, David M. Lawrence, Carolyn Gibson, and A. Britta K. Sannel. 2019. "Permafrost Collapse Is Accelerating Carbon Release." *Nature*, 569(7754): 32–34. 12

Van den Bremer, Ton S., and Frederick Van der Ploeg. 2021. "The Risk-Adjusted Carbon Price." *American Economic Review*, 111(9): 2782–2810. 5

Van der Ploeg, Frederick, and Aart De Zeeuw. 2018. "Climate Tipping and Economic Growth: Precautionary Capital and the Price of Carbon." *Journal of the European Economic Association*, 16(5): 1577–1617. 5

Van Westen, René M., Michael Kliphuis, and Henk A. Dijkstra. 2024. "Physics-Based Early Warning Signal Shows That AMOC Is on Tipping Course." *Science Advances*, 10(6): eadk1189. 13

Wagener, Florian. 2013. "Regime Shifts: Early Warnings." In *Encyclopedia of Energy, Natural Resource, and Environmental Economics*. 349–359. Elsevier. 6, 13

Wagener, Florian. 2015. "Economics of Environmental Regime Shifts." In *The Oxford Handbook of the Macroeconomics of Global Warming*. , ed. Lucas Bernard and Willi Semmler, 0. Oxford University Press. 6

A Calibration and Parameters

A.1 Climate Model

This section discusses the calibration of the climate model. The optimisation of differential equations parameters is done via the `SciMLSensitivity.jl` and `Optim` packages (Rackauckas et al., 2020). The baseline year $t = 0$ of the calibration is chosen to be 2020. The calibration horizon is of $\tau = 130$ years, such that the calibration matches variables through 2150.

A.1.1 Greenhouse Gasses Emissions under No-Policy

I assume the emission of greenhouse gasses (GHGs) in the no-policy (np) scenario follows the median path in the SSP5-8.5 scenario, sourced from the CMIP6 GHG and aerosol emission project (Gidden et al., 2019). First, I extract median paths $\hat{M}^{np}_{c,t}$ in p.p.m. of five major GHGs

$$c \in \{ \mathrm{CO_2},\ \mathrm{CH_4},\ \mathrm{N_2O},\ \mathrm{NF_3},\ \mathrm{SF_6}\}.$$

Finally, I construct the no-policy path of the $\mathrm{CO_2e}$ atmospheric concentration as

$$\hat{M}^{np}_{t} = \hat{M}^{np}_{\mathrm{CO_2},t} + \sum_{c} \mathrm{GWP}_c \times \hat{M}^{np}_{c,t}, \tag{32}$$

where GWP_c is the Global Warming Potential of the GHG c, as provided in the AR6, Working Group I from the IPCC (2023*a*). These are summarised in table 1. Figure 16 illustrates the fraction of atmospheric $\mathrm{CO_2}$ concentration $\hat{M}^{np}_{t,\,\mathrm{CO_2}}$

GHG c	GWP
$\mathrm{CH_4}$	29.8
$\mathrm{N_2O}$	273
$\mathrm{NF_3}$	17400
$\mathrm{SF_6}$	24300

Table 1: Global Warming Potential used in the calibration.

to the fraction of the $\mathrm{CO_2e}$ atmospheric concentration $\hat{M}^{np}_{t}$ (32). Given this

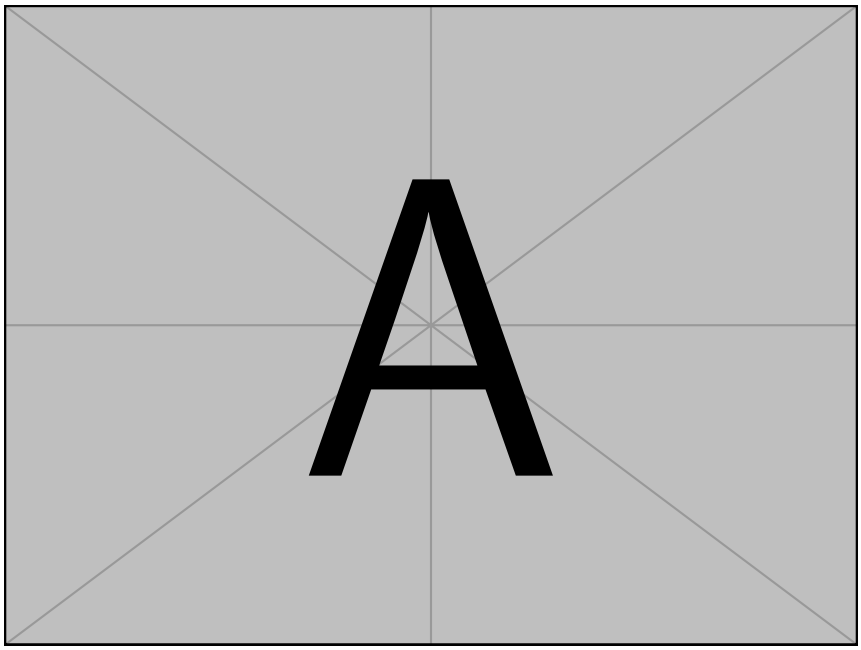

Figure 16: Fraction of $\mathrm{CO_2}$ to $\mathrm{CO_2e}$ concentration, $\hat{M}^{np}_{t,\,\mathrm{CO_2}}/\hat{M}^{np}_t$

calibration, around 18% of radiative forcing in 2020 is due to non- $\mathrm{CO_2}$ GHGs. Later in the century, $\mathrm{CO_2}$ becomes a larger contributor of radiative forcing, as the emissions of all GHGs tend to fall and $\mathrm{CO_2}$ has a longer half-life of other GHGs.

For tractability, I further estimate the growth rate γ^{np}_t (3) of $\mathrm{CO_2e}$ concentration M^{np}_t by assuming it to be a polynomial function of time as

$$\gamma^{np}_t = \sum_{n=0}^{k} c_n t^n \tag{33}$$

and estimate the parameters $\{c_n\}_n$ and the order k to minimise the error between the calibrated $\mathrm{CO_2e}$ concentration $M^{np}_t = M_0 e^{\int_0^\tau \gamma^{np}_t \mathrm{d}t}$ and the path of $\mathrm{CO_2e}$ concentration $\hat{M}^{np}_t$ implied in Gidden et al. (2019), over the horizon τ, and a penalty term for the order k, that is,

$$(k, \{c_n\}_n) = \arg\min_{k,\{c_n\}_n} \int_0^\tau |M^{np}_t - \hat{M}^{np}_t|^2 \mathrm{d}t + \lambda k^2. \tag{34}$$

The resulting order k and coefficients $\{c_n\}_n$ are displayed in Table 2 and the calibrated γ^{np}_t and M^{np}_t are illustrated in Figure 1. The calibration's maximal

	Calibrated Value
k	4
c_0	-0.0001730
c_1	-0.09061
c_2	0.0001288
c_3	$-6.10\text{e}{-8}$
c_4	$9.61\text{e}{-12}$

Table 2: Calibrated parameters k and $\{c_n\}_n$ for the growth rate γ_t^{np} (33) of M_t^{np}.

absolute error $\max_t |M_t^{np} - \hat{M}_t^{np}|$ is 0.009785412 p.p.m..

A.1.2 Temperature in Absence of Tipping Elements

I calibrate GHG forcing g (10) to match the mapping between GHG and temperature in the FaIRv2 model developed by Leach et al. (2021). I choose this model to be consistent with the dynamics in Deutloff, Held and Lenton (2025), which is then used to calibrate the temperature impact of tipping elements. First, I divide the calibration period $[0, \tau]$ into an estimation period $[0, 80]$ of 80 years and an out-of-sample testing period $[80, \tau]$. Second, I simulate the path of CO_2e carbon concentration M_t^{np} under the no-policy scenario np using the FaIRv2 model. Third, I generate a probabilistic projection of temperature deviations from pre-industrial levels under M_t^{np} and extract the median temperature path $\hat{T}_t^{np}$. Finally, assuming no positive-feedback in temperature (9), that is, $\lambda(T_t) \equiv \lambda_1$, I calibrate the GHGs forcing parameters G_0, G_1, in g (10) to minimise the resulting median temperature path simulated under the temperature dynamics (11), that is,

$$(G_0, G_1) = \arg\min_{G_0, G_1} \int_0^{80} |T_t^{np} - \hat{T}_t^{np}|^2 \mathrm{d}t. \tag{35}$$

The calibration targets the median path of temperature from FaIRv2 as the uncertainty in the FaIRv2 projections of temperature is mostly due to uncertainty in models and in emissions, rather than to yearly temperature variability. See Guivarch et al. (2022) for a detailed discussion. The calibrated parameters are reported in Table 3 and the resulting median temperature dynamics T_t^{np} are

shown in Figure 17. The calibration maximal absolute error $\max_t |T_t^{np} - \hat{T}_t^{np}|$ is

	Calibrated Value	Description
G_0	150.424	Intercept
G_1	22.687	Slope

Table 3: Calibrated parameters G_0 and G_1 for the CO_2e forcing (10).

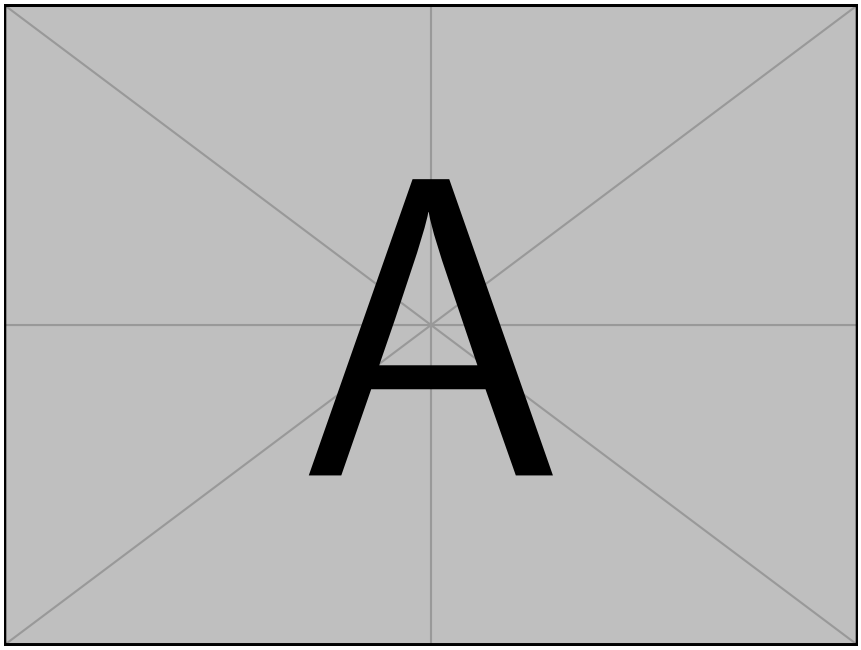

Figure 17: Median calibrated temperature T_t^{np} path and the target FaIRv2 temperature projections $\hat{T}_t^{np}$ with 95% confidence intervals.

0.05705 °C in the estimation period and 0.23766 °C out of sample.

I further validate the calibration by simulating the impulse response of temperature to a one-off increase of CO_2e concentration of 47 p.p.m. and compute the time it takes median temperature to reach half way to its equilibrium level, defined as "half-life" in Dietz et al. (2021*a*). The median half-life in the calibrated model is approximately 6 months, which is faster than the approximately 3 years FaIRv2 model. Despite this large error, the model still performs better than many models commonly employed in the IAM literature (e.g. DICE2016), which display a very sluggish response of temperature to CO_2e (Dietz et al., 2021*a*).

A.1.3 Temperature Impact of Tipping Elements

The impact of temperature feedbacks on temperature is calibrated from Deutloff, Held and Lenton (2025), hereafter DHL. The critical temperatures of the feedback mechanisms, T^c in the context of my model, are chosen by DHL to be the central estimates of Armstrong McKay et al. (2022). Given the wide uncertainty in these estimates, here I consider a more robust, albeit prudent approach, by not calibrating T^c and computing the regret for various values of the critical temperature. Hence, I rely on DHL to match only the impact on temperature, and not the timing, of the feedback mechanisms. The transition function $L(T_t - T^c)$ of the feedback mechanism (8) takes the form[7]

$$L(T_t - T^c) = \frac{1}{1 + \exp\left(L_1\left(T_t - T^c\right) + L_0\right)}. \tag{36}$$

I calibrate the parameters $\Delta\lambda$, L_0, and L_1 by matching the additional warming at the end of the century between the DHL model with temperature feedbacks ("coupled") and without temperature feedbacks ("uncoupled"). More formally, introduce the radiative forcing

$$r^l(T_t) \coloneqq S_0\left(1 - \lambda_1\right) - \eta\sigma T_t^4 \tag{37}$$

in absence of positive temperature feedbacks and $T_t^{l,np}$ the temperature path satisfying (11) with radiative forcing (37) under the np scenario. Then, the impact of temperature feedbacks on the end-of-century is defined as

$$\Delta T^{np} = T_{2100}^{np} - T_{2100}^{l,np}. \tag{38}$$

Then the parameters $\Delta\lambda$, L_0, and L_1 are chosen to minimise the square distance of the median, 5% and 95% quantiles between ΔT^{np} and the DHL additional warming $\hat{\Delta T}^{np}$. The results of the calibration are provided in Table 4.

[7] See Bondarev and Greiner (2018) for a discussion on the effect of an alternative specification on the results of the optimisation problem.

	Calibrated Value	Description
L_0	3.15	Location Parameter
L_1	3.5 $[°C^{-1}]$	Speed Parameter
λ_1	0.31	Initial level of feedback
ΔS	0.01545 $[Wm^{-2}]$	Magnitude of feedback

Table 4: Calibration of feedback mechanism (36).

A.1.4 Other Climate Parameters

The remaining parameters of the climate model are reported in Table 5.

Climate		
T_0	1.34 $[°C]$	Initial temperature
M_0	558.75 [p.p.m.]	Initial CO_2e concentration
M^p	383.15 [p.p.m.]	Pre-industrial CO_2e concentration
N_0	286.66 [p.p.m.]	Initial CO_2e concentration equivalent in sinks
σ_T	1.5844 $[y^{-1/2}]$	Volatility of temperature
S_0	340.5 $[W\,m^{-2}]$	Mean solar radiation
ϵ	15.844 $[J\,m^{-2}\,K\,y]$	Heat capacity of the ocean
η	5.67e−8	Stefan-Boltzmann constant

Table 5: Remaining parameters of the climate model.

A.2 Economy

A.2.1 Preferences

The following Table 6 illustrates the preferences parameters used throughout the paper. There is no consensus in the literature on preference parameters. In line with previous literature focusing on recursive preferences, I set relative risk aversion $\theta = 10$ (Ackerman, Stanton and Bueno, 2013; Crost and Traeger, 2013; Lontzek et al., 2015) and the time preference parameter $\rho = 1.5\%$ (Nordhaus,

2014). Following the discussion in Hambel, Kraft and Schwartz (2021), I choose $\psi = 1$.

Preferences		
ρ	1.5%	Time preference
θ	10	Relative risk aversion
ψ	1	Elasticity of intertemporal substitution

Table 6: Parameters of preferences.

A.2.2 Marginal Abatement Curves

The function β'_t (20) is calibrated to match the implied marginal abatement curves in the Sixth Assessment Report of the IPCC (2023*b*, Figure 3.33). The data is sourced from Byers et al. (2022). In the model, the marginal abatement cost $\mathrm{MAC}_t := -\frac{\partial B_t}{\partial E_t}$ can be linked to β' via a straightforward calculation, that is,

$$\beta'_t = \mathrm{MAC}_t \frac{E_t^{\mathrm{np}}}{Y_t}. \tag{39}$$

For each SSP scenario and each IAM m in the dataset, I extract carbon prices, which are assumed to be equal to marginal abatement costs $\mathrm{MAC}_{m,t}$, emission $E_{m,t}$, baseline emissions $E_{m,t}^{\mathrm{np}}$, and output $Y_{m,t}$. Then, I compute the implied

$$\beta'_{m,t} = \mathrm{MAC}_{m,t} \frac{E_{m,t}^{\mathrm{np}}}{Y_{m,t}} \tag{40}$$

and

$$\varepsilon_{m,t} = 1 - \frac{E_{m,t}}{E_{m,t}^{\mathrm{np}}}. \tag{41}$$

Then, I compute for $t = 0$ the power b that minimises the mean-squared error $\beta'_{m,0} = \log(b\omega_0) + (b-1)\log\varepsilon_{m,0}$. Finally, I estimate via linear regression, for each model m, the coefficients $\alpha_{m,0}$ and $\alpha_{m,1}$ of

$$\log\beta'_{m,t} - \log b - (b-1)\log\varepsilon_{m,t} = \alpha_{m,0} + \alpha_{m,1}t, \tag{42}$$

noticing that these can be related, via the abatement technology parameter ω_t (21), to the parameters of interest

$$\omega_0 = \log(\alpha_{m,0}), \tag{43}$$

$$\rho_\omega = -\alpha_{m,1}. \tag{44}$$

This procedure yields the estimates in Table 7. In the paper, the estimates used

Model m	ω_0		ρ_ω	
IMAGE	0.0532	(0.003298)	0.0045	(0.000023)
WITCH-GLOBIOM	0.0633	(0.002079)	-0.0215	(0.000014)
AIM/CGE	0.0560	(0.002265)	0.0071	(0.000017)

Table 7: Estimated β' parameters for each model m. Standard errors in parentheses.

are those of the IMAGE model, that is,

$$\omega_0 = 5.32\%, \rho_\omega = 0.45\% \text{ and } b = 2.8. \tag{45}$$

A.2.3 Damage Function

Most integrated assessment models, including the one presented in this paper, summarise the effect of an increase in global average temperatures as a simple damage function d. Despite its convenience, there is no broad consensus on whether damages ought to be a function of temperature T_t or temperature changes $\mathrm{d}T_t$, the form this function should take, and whether the damages should affect output Y_t or output growth $\mathrm{d}Y_t$. For an overview on this debate, I refer the reader to the surveys by Howard and Sterner (2017), Nordhaus and Moffat (2017), and Tol (2024). In this paper, I follow recent evidence on the effect of temperature T_t on productivity growth $\mathrm{d}A_t$ (Burke, Hsiang and Miguel, 2015; Dell, Jones and Olken, 2012; Kalkuhl and Wenz, 2020), and assume that climate damages d_t at time t lower the growth rate of productivity

$$\frac{\mathrm{d}A_t}{\mathrm{d}t} = \varrho - d_t. \tag{46}$$

I employ the calibration by Kalkuhl and Wenz (2020). The authors estimate the quadratic cumulative damages of warming since pre-industrial on cumulative loss in GDP growth, equivalent to the formulation used in Burke, Hsiang and Miguel (2015). The estimated parameter is $\xi = 0.0709\%$.

A.2.4 Macroeconomy

For the remaining calibration of the economy (Table 8), I follow the calibration suggested by Hambel, Kraft and Schwartz (2021, Section 3). I first calibrate the expected growth rate $\varrho + \phi(\chi_t)$ of output (23) in absence of abatement measures to match the DICE model through 2200. As in Hambel, Kraft and Schwartz (2021), as DICE is deterministic, I match the average simulation of my model to the DICE output. Following Pindyck and Wang (2013), the initial level of productivity is set at $A(0) = 0.113$.

Economy		
ω_0	11%	GDP loss required to fully abate today
ρ_ω	2.7%	Rate of abatement cost reduction
ϱ	0.09% $[\mathrm{y}^{-1}]$	Growth of TFP
κ	6.32% $[\mathrm{y}^{-1}]$	Adjustment costs of abatement technology
δ_k	0.0116 $[\mathrm{y}^{-1}]$	Initial depreciation rate of capital
ξ	$2.6\mathrm{e}{-4}$ $[^\circ\mathrm{C}^{-\nu}\mathrm{y}^{-1}]$	Coefficient of damage function
ν	3.25	Exponent of damage function
A_0	0.113	Initial TFP
Y_0	75.8 [trUS\$/y]	Initial GDP
σ_k	0.0162 $[\mathrm{y}^{-1/2}]$	Variance of GDP
τ	500 [y]	Steady state horizon

Table 8: Parameters of the economic model.

B Numerical Solution of Climate-Economy Model

This appendix deals with the solution of the maximisation problem (25).

The numerical solution relies on three steps. First, in Section B.1, I make some simplifying assumption on the decay rate of carbon δ_m. This allows to drop the carbon stored in sinks N_t from the state space. Second, in Section B.2, I use this assumption to derive a Hamilton-Jacobi-Bellman partial differential equation for the value function of the social planner V (25). Third, in Section B.3, I derive an approximating Markov chain, that is, a discretisation of the state space and a discrete Markov chain over it, which converges to the Hamilton-Jacobi-Bellman equations. This extends the techniques developed by Kushner and Dupuis (2001) and Kushner (2007) to a problem with recursive utility, such as the ones solved in Sections 3. I further provide a parallelisation technique based on Bierkens, Fearnhead and Roberts (2019).

B.1 Simplifying Assumptions on the Decay Rate of Carbon

Following Hambel, Kraft and Schwartz (2021), I make an assumption on the decay rate of carbon. The calibrated carbon decay δ_m, as a function of the carbon stored in sinks N_t. The calibration assumes a functional form

$$\delta_m(N_t) = a_\delta e^{-\left(\frac{N_t - c_\delta}{b_\delta}\right)^2}, \tag{47}$$

for parameters $a_\delta, b_\delta, c_\delta$. I assume that the amount of carbon sinks present in the atmosphere is a constant fraction of the concentration in the atmosphere, $N_t = \frac{N_0}{M_0} M_t$. Abusing notation, I henceforth write $\delta_m(M_t)$ for the decay rate. Using this setup, under a no-policy scenario, the decay of carbon follows the path in Figure 18.

B.2 Hamilton-Jacobi-Bellman equation

This section derives the Hamilton-Jacobi-Bellman (HJB) equation for the social planner problem and the emission game.

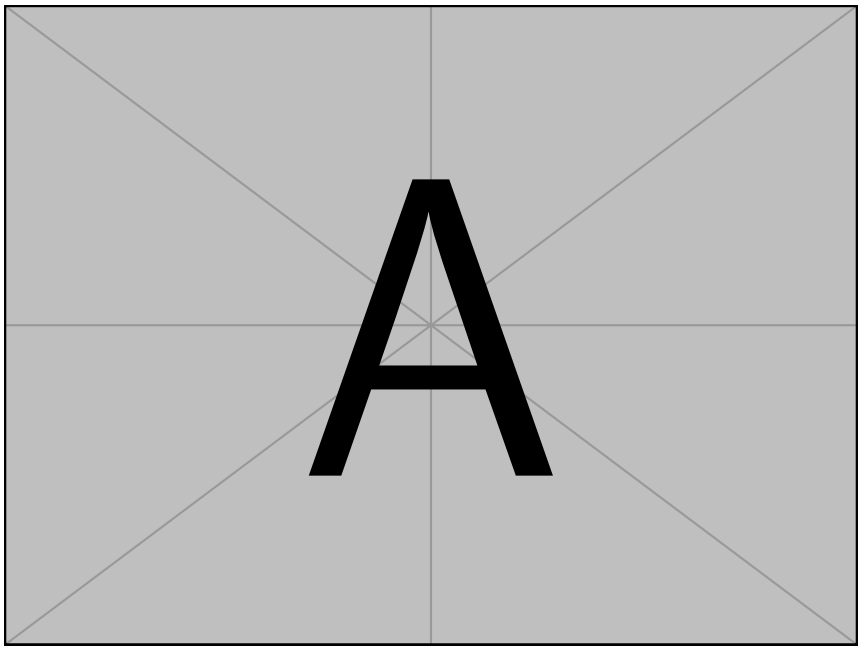

Figure 18: Estimated decay of carbon δ_m under the no-policy emission scenario M^{np}.

B.2.1 Hamilton-Jacobi-Bellman equation

The value function of the social planner V (25) at time t depends only on temperature T_t, log-CO_2e concentration m_t and output Y_t. This satisfies the HJB equation

$$\begin{aligned} -\partial_t V = \sup_{\chi,\alpha} & f(\chi Y, V) + \partial_m V \ (\gamma_t^{\text{np}} - \alpha) + \partial_m^2 V \ \frac{\sigma_m^2}{2} \\ & + \partial_Y V(\varrho + \phi(\chi) - d(T,m) - \beta_t(\varepsilon(\alpha)))Y + \partial_Y^2 V \ \frac{\sigma_Y^2}{2} Y^2 \\ & + \partial_T V \ \frac{r(T) + g(m)}{\epsilon} + \partial_T^2 V \ \frac{(\sigma_T/\epsilon)^2}{2}. \end{aligned} \tag{48}$$

Now, I derive an auxiliary, lower dimensional HJB equation using the ansatz

$$V_t(T, m, Y) \equiv \frac{Y^{1-\theta}}{1-\theta} F(T, m). \tag{49}$$

First, I compute the Epstein-Zin aggregator at the ansatz $V \equiv F\frac{Y^{1-\theta}}{1-\theta}$. Recall that

the Epstein-Zin aggregator is given by

$$f(\chi Y, V) \coloneqq \rho \frac{(1-\theta)\, V}{1-1/\psi} \left(\left(\frac{\chi Y}{((1-\theta)V)^{\frac{1}{1-\theta}}} \right)^{1-1/\psi} - 1 \right). \tag{50}$$

Notice that

$$(1-\theta)V = FY^{1-\theta} \tag{51}$$

$$((1-\theta)V)^{\frac{1}{1-\theta}} = F^{\frac{1}{1-\theta}} Y. \tag{52}$$

Plugging back into the aggregator we obtain

$$f(\chi Y, V) = Y^{1-\theta} \, \frac{\rho F}{1-1/\psi} \left(\left(\frac{\chi}{F^{\frac{1}{1-\theta}}} \right)^{1-1/\psi} - 1 \right). \tag{53}$$

Hence, f is homogenous of degree $1-\theta$ in Y. Second, we can evaluate the derivates of the value function at our ansatz

$$\begin{aligned}
\partial_Y V &= Y^{-\theta} F, \qquad \partial_Y^2 V = -\theta Y^{-\theta-1} F, \\
\partial_T V &= \frac{Y^{1-\theta}}{1-\theta} \, \partial_T F, \; \partial_T^2 V = \frac{Y^{1-\theta}}{1-\theta} \, \partial_T^2 F, \\
\partial_m V &= \frac{Y^{1-\theta}}{1-\theta} \, \partial_m F, \; \partial_m^2 V = \frac{Y^{1-\theta}}{1-\theta} \, \partial_m^2 F, \\
\partial_t V &= \frac{Y^{1-\theta}}{1-\theta} \, \partial_t F.
\end{aligned}$$

Plugging this into the HJB equation we obtain

$$
\begin{aligned}
-\frac{Y^{1-\theta}}{1-\theta}\partial_t F = \sup_{\chi,\alpha}\Bigg\{ & Y^{1-\theta}\frac{\rho F}{1-1/\psi}\left(\left(\frac{\chi}{F^{1/(1-\theta)}}\right)^{1-1/\psi}-1\right) \\
& + \frac{Y^{1-\theta}}{1-\theta}\partial_m F(\gamma_t^{\mathrm{np}}-\alpha) + \frac{Y^{1-\theta}}{1-\theta}\partial_m^2 F\frac{\sigma_m^2}{2} \\
& + Y^{-\theta}F\left(\varrho+\phi(\chi)-d(T,m)-\beta_t(\varepsilon(\alpha))\right)Y \\
& - \theta Y^{-\theta-1}F\frac{\sigma_Y^2}{2}Y^2 \\
& + \frac{Y^{1-\theta}}{1-\theta}\partial_T F\frac{r(T)+g(m)}{\epsilon} + \frac{Y^{1-\theta}}{1-\theta}\partial_T^2 F\frac{(\sigma_T/\epsilon)^2}{2}\Bigg\}
\end{aligned}
\tag{54}
$$

Dividing both sides by $\frac{Y^{1-\theta}}{1-\theta}$, we obtain

$$
\begin{aligned}
-\partial_t F = \inf_{\chi,\alpha}\Bigg\{ & (1-\theta)\frac{\rho F}{1-1/\psi}\left(\left(\frac{\chi}{F^{1/(1-\theta)}}\right)^{1-1/\psi}-1\right) \\
& + (1-\theta)F\left(\varrho+\phi(\chi)-d(T,m)-\beta_t(\varepsilon(\alpha))-\theta\frac{\sigma_Y^2}{2}\right) \\
& + \partial_m F(\gamma_t^{\mathrm{np}}-\alpha) + \partial_m^2 F\frac{\sigma_m^2}{2} \\
& + \partial_T F\frac{r(T)+g(m)}{\epsilon} + \partial_T^2 F\frac{(\sigma_T/\epsilon)^2}{2}\Bigg\}.
\end{aligned}
\tag{55}
$$

B.2.2 Unitary Elasticity of Intertemporal Substitution $\psi \to 1$

Using the fact that

$$
\begin{aligned}
\lim_{\psi\to 1}\frac{\rho F}{1-1/\psi}\left(\left(\frac{\chi}{F^{1/(1-\theta)}}\right)^{1-1/\psi}-1\right) &= \rho F\ln\left(\frac{\chi}{F^{1/(1-\theta)}}\right) \\
&= \rho F\left(\ln(\chi)-\frac{\ln(F)}{1-\theta}\right)
\end{aligned}
\tag{56}
$$

we obtain a simplified HJB

$$
\begin{aligned}
-\partial_t F = \inf_{\chi,\alpha} \Bigg\{ & (1-\theta)\,\rho F \ln(\chi) - \rho F \ln(F) \\
& + (1-\theta) F \left(\varrho + \phi(\chi) - d(T,m) - \beta_t(\varepsilon(\alpha)) - \theta \frac{\sigma_Y^2}{2} \right) \\
& + \partial_m F (\gamma_t^{\text{np}} - \alpha) + \partial_m^2 F \frac{\sigma_m^2}{2} \\
& + \partial_T F \frac{r(T) + g(m)}{\epsilon} + \partial_T^2 F \frac{(\sigma_T/\epsilon)^2}{2} \Bigg\}.
\end{aligned} \tag{57}
$$

Introduce the change of variable $H \coloneqq \log(F)$, such that

$$
\begin{aligned}
\frac{\partial_t F}{F} &= \partial_t H, \\
\frac{\partial_T F}{F} &= \partial_T H, \quad \frac{\partial_T^2 F}{F} = (\partial_T H)^2 + \partial_T^2 H, \\
\frac{\partial_m F}{F} &= \partial_m H, \quad \frac{\partial_m^2 F}{F} = (\partial_m H)^2 + \partial_m^2 H.
\end{aligned}
$$

Using the change of variables we can rewrite (57) we can rewrite

$$
\begin{aligned}
\rho H - \partial_t H = \inf_{\chi,\varepsilon} \Bigg\{ & (1-\theta) \left(\rho \ln(\chi) + \varrho + \phi(\chi) - d(T,m) - \frac{\omega_t}{2}\varepsilon^2 - \theta \frac{\sigma_Y^2}{2} \right) \\
& + (\gamma_t^{\text{np}} - (\gamma_t^{\text{np}} + \delta_m(m))\,\varepsilon) \partial_m H + \frac{\sigma_m^2}{2} \left((\partial_m H)^2 + \partial_m^2 H \right) \\
& + \frac{r(T) + g(m)}{\epsilon} \partial_T H + \frac{(\sigma_T/\epsilon)^2}{2} \left((\partial_T H)^2 + \partial_T^2 H \right) \Bigg\}.
\end{aligned} \tag{58}
$$

B.2.3 First Order Conditions

Under unitary elasticity of intertemporal substitution $\psi \to 1$, the optimal policy rates can be determined analytically

$$
\chi_t^* = \frac{\kappa A_t - 1 + \sqrt{(\kappa A_t - 1)^2 + 4\kappa\rho}}{2\kappa A_t} \text{ and } \varepsilon_t^* = -\frac{\gamma_t^{np} + \delta_m(m)}{\omega_t (1-\theta)}\, \partial_m H. \tag{59}
$$

Using this, (58) can be further simplified to

$$\begin{aligned}\rho H - \partial_t H = (1-\theta)\left(\rho \ln(\chi_t^*) + \varrho + \phi(\chi_t^*) - d(T,m) - \theta\frac{\sigma_Y^2}{2}\right) \\ + \frac{r(T)+g(m)}{\epsilon}\partial_T H + \gamma_t^{np}\partial_m H \\ + \frac{1}{2}\left(\sigma_m^2 + \frac{\left(\gamma_t^{np} + \delta_m(m)\right)^2}{\omega_t(1-\theta)}\right)(\partial_m H)^2 + \frac{\sigma_m^2}{2}\partial_m^2 H \\ + \frac{(\sigma_T/\epsilon)^2}{2}\left((\partial_T H)^2 + \partial_T^2 H\right).\end{aligned} \tag{60}$$

B.3 Approximating Markov Chain

The objective is to solve for the function F by adapting the method proposed in Kushner and Dupuis (2001) and Kushner (2007). I discretise the state space of temperature T and $\mathrm{CO_2e}$ log-concentration m by a fixed grid of size parametrised by some small step size h. I discretise the time t by computing state dependent intervals $\Delta t(T,m)$. Then I define a Markov chain $\mathcal{M}$ over the discretised space. Finally, I compute a discretised value function $F^h : \mathcal{X} \to \mathcal{X}$ with the property that

$$\sup_{x\in\mathcal{X}} |F^h(x) - F(x)| \to 0 \text{ as } h \to 0, \tag{61}$$

for any compact subset $\mathcal{X} \subset [T^p, \infty) \times [m^p, \infty) \times [0, \infty)$. For more details on convergence, see Chapter 15 of Kushner and Dupuis (2001).

First, I fix a suitable subset of the state space

$$\mathcal{X} := [T^p, T^p + \Delta T] \times [m^p, m^p + \Delta m]. \tag{62}$$

In practice ΔT and Δm are chosen such that T in the upper-right corner of the grid, the drift $\mu(T^p + \Delta T, m^p + \Delta m) \equiv 0$. Then, given a step size $h > 0$ I define the grid over the space $\mathcal{X}$ by

$$\begin{aligned}\Omega_h(\mathcal{X}) = (T^p, T^p + h\Delta T, \ldots, T^p + (1-h)\Delta T, T^p + \Delta T) \times \\ (m^p, m^p + h\Delta m, \ldots, m^p + (1-h)\Delta m, m^p + \Delta m).\end{aligned} \tag{63}$$

Using the ansatz (49) I now define a discretised value function F_t^h over the grid such that $F_t^h \to F$ as $h \to 0$. First, introduce the discrete-time Epstein-Zin aggregator

$$J^h(\chi, F) = \left(\left(1 - e^{-\rho\Delta t}\right) \chi^{1-\frac{1}{\psi}} + e^{-\rho\Delta t} \left(\delta_y(\chi) F\right)^{\frac{1-\frac{1}{\psi}}{1-\theta}} \right)^{\frac{1-\theta}{1-\frac{1}{\psi}}}, \tag{64}$$

where

$$\begin{aligned} \delta_y(\chi) &:= \mathbb{E}_t \left[\left(\frac{Y_{t+\Delta t}}{Y_t} \right)^{1-\theta} \right] \\ &= 1 + \Delta t(1-\theta) \left(\varrho + \phi(\chi) - d(T_t) - \frac{\theta}{2}\sigma_k^2 \right) + \mathbb{E}_t \mathcal{O}\left(\Delta t^{\frac{3}{2}}\right). \end{aligned} \tag{65}$$

As the aggregator J^h satisfies Assumptions 1 through 4 of Kraft and Seifried (2014, p. 534), we have uniform convergence of the discrete-time operator to the continuous analogue, that is,

$$\sup_{F \in \mathcal{F}, \chi \in \mathcal{C}} \left| \frac{J^h(\chi, F) - J(\chi, F)}{h} - g(\chi, F) \right| \to 0 \text{ as } h \to 0, \tag{66}$$

for each compact $\mathcal{F} \subset \mathbb{R}$ and $\mathcal{C} \subseteq [0, 1]$. The discretised value function satisfies the recursion

$$F^h(T_t, m_t) = \min_{\chi, \alpha} J^h\left(\chi, \mathbb{E}_{t, \mathcal{M}(\alpha)} F_{t+\Delta t}(T_t, m_t)\right), \tag{67}$$

where $\mathbb{E}_{t,\mathcal{M}(\alpha)}$ is the expectation with respect to the Markov chain $\mathcal{M}(\alpha)$ over the grid $\Omega_h(\mathcal{X})$. The Markov chain $\mathcal{M}(\alpha)$, parameterised by h, is constructed as follows. Introduce the normalising factor

$$Q_t(T, m, \alpha) := \left(\frac{\sigma_T}{\epsilon \Delta T}\right)^2 + \left(\frac{\sigma_m}{\Delta m}\right)^2 + h \left| \frac{r(T) + g(m)}{\epsilon \Delta T} \right| + h \left| \frac{\gamma_t^{\text{np}} - \alpha}{\Delta m} \right|. \tag{68}$$

Then the probabilities of moving from a point $(T, m) \in \Omega_h(\mathcal{X})$ of the grid to an

adjacent point are given by

$$p(T \pm h\Delta T, m \mid T, m) \propto \frac{1}{2}\left(\frac{\sigma_T}{\epsilon \Delta T}\right)^2 + h\left(\frac{r(T) + g(m)}{\epsilon \Delta T}\right)^{\pm} \text{ and} \tag{69}$$

$$p(T, m \pm h\Delta m \mid T, m) \propto \frac{1}{2}\left(\frac{\sigma_m}{\Delta m}\right)^2 + h\left(\frac{\gamma_t^{\mathrm{np}} - \alpha}{\Delta m}\right)^{\pm} \tag{70}$$

where $(\cdot)^+ \coloneqq \max\{\cdot, 0\}$ and $(\cdot)^- \coloneqq -\min\{\cdot, 0\}$. One can check that this is a well-defined probability measure. Finally, the time step is given by

$$\Delta t = h^2 / Q_t(T, m, \alpha), \tag{71}$$

which satisfies $\Delta t \to 0$ as $h \to 0$.

The Markov chain defined above allows us to derive $F_t^h(T_t, m_t)$ from the subsequent $F_{t+\Delta t}^h(T_{t+\Delta t}, m_{t+\Delta t})$. This requires a terminal condition

$$\bar{F}^h(T_\tau, m_\tau) \coloneqq F_\tau^h(T_\tau, m_\tau). \tag{72}$$

To derive this, assume that at some point in a far future $\tau \gg 0$, the abatement is free and all emissions are abated, $\gamma^{\mathrm{np}} \equiv \alpha$ for the social planner such that $\mathrm{d}m \equiv \sigma_m \mathrm{d}W_m$. Then I construct an equivalent, control independent, Markov chain $\bar{\mathcal{M}}$ as above for the steady state value function

$$\bar{F}^h(T, m) = \min_{\chi} J^h\left(\mathbb{E}_{t,\bar{\mathcal{M}}} \bar{F}(T, m); \chi\right). \tag{73}$$

This is now a fixed point equation for $\bar{F}$ which can be solved by value or policy function iteration. As the abatement control is bounded, $|\alpha_t| \leq \gamma_t^{\mathrm{np}}$ the controlled drift

$$\begin{pmatrix} \mu(T_t, m_t) & \alpha_t - \gamma_t^{\mathrm{np}} \end{pmatrix} \tag{74}$$

of the state vector (T_t, m_t) is also bounded, as well as continuous in the state vector. Furthermore, the aggregator J^h is bounded and continuous. This implies that the problem at hand satisfies Assumptions 10.1.1 and 10.1.2 for (weak) convergence given in Kushner and Dupuis (2001, p. 269). Hence, we have con-

vergence of the discretised value function to the continuous analogue, $\bar{F}^h \to \bar{F}$. The steady state value function $\bar{F}$ serves then as a continuous and bounded terminal condition of the finite horizon problem (67). Which, in turn, implies (weak) convergence of $F_t^h \to F$ as $h \to 0$.

B.3.1 Convergence of Numerical Method

The convergence of the steady state HJB equation (73) for $\bar{F}$ is achieved via iterated application of the right-hand side. As J is contracting, repeated application is guaranteed to converge to the unique fixed point $\bar{F}^h$. Convergence is determined when the absolute and relative tolerance both fall below than 1×10^{-7} and 1×10^{-8} respectively. The convergence values are shown below 9. To check the robustness of the convergence procedure, I also computed the

T^c	Iterations	Abs. Tolerance	Policy error with $h/2$
Linear	8950	9.96×10^{-8}	1.345×10^{-3}
2°	9441	9.9972×10^{-8}	2.268×10^{-3}
3°	9449	9.9973×10^{-8}	2.593×10^{-3}
4°	9440	9.9972×10^{-8}	2.113×10^{-3}

Table 9: Convergence metrics for different critical thresholds with $h = 4 \times 10^{-3}$. The policy error is the absolute difference in policy for a denser grid $h/2$.

terminal value function and policy on a denser grid with step size by $h/2$ and check the maximum absolute error on the coarser grid. These are reported in the fourth column.

Furthermore, I employ a verification test based on Oberkampf and Roy (2010), as in Cai and Lontzek (2019). I consider a determnistic model $\sigma_m = \sigma_T = 0$, such that the HJB equation (58) can be solved via a upwind-downwind finite-difference scheme. The solution of the latter is then compared to the solution of the approximating Markov Chain method described above. The error between the two methods is displayed in Table 10.

T^c	Abs. Error
Linear	4.2×10^{-4}
2°	7.1×10^{-3}
3°	8.2×10^{-3}
4°	8.7×10^{-3}

Table 10: Absolute error in the value function for H computed via an approximating Markov chain and an upwind-downwind finite-difference scheme.

B.4 Parallelisation

When computing the backward recurrence (67), conditional on a given strategy α, each grid point $X_i \in \Omega^h(\mathcal{X})$ is assigned a different time step $\Delta t(X_i; \alpha)$, which depends on the curvature of the drift at that state. To parallelise the computation, I leverage the ZigZag algorithm by Bierkens, Fearnhead and Roberts (2019). Given the value function F_t^h, for a step back $t - \min_i \Delta t(X_i; \alpha)$, I construct a directed graph among grid points $\mathcal{X}$ where an edge $X_i \to X_j$ is drawn if there is a positive probability of transitioning from X_i to X_j under the Markov Chain $\mathcal{M}$. This allows to obtain, at each point in time t, sets of points $\mathcal{C}_t \subseteq \mathcal{X}$ which are independent and over which it is possible to parallelise. The parallelisation has been conducted on Snellius, the national high performance computer of the Netherlands. The algorithm is written in the `Julia` programming language and relies on `Optim.jl` developed by Mogensen and Riseth (2018) and the differential equation suit developed by Rackauckas and Nie (2017).